# Synthesis and Characterization of Cobalt and Nickel Doped in Barium Hexaferrite Nanoparticles for Photocatalysis

**By**

**Muhammad Jahanzaib**

**School of Chemical and Materials Engineering**

**National University of Sciences and Technology**

**2021**

# Synthesis and Characterization of Cobalt and Nickel Doped in Barium Hexaferrite Nanoparticles for Photocatalysis

Names: Muhammad Jahanzaib

Reg.No:0000-205655

**This thesis is submitted as a partial fulfillment of the requirements for the degree of MS in Nanoscience and Engineering**

**Supervisor Name: Dr. Iftikhar Hussain Gul**

**School of Chemical and Materials Engineering (SCME)**

**National University of Sciences and Technology (NUST)**

**H-12 Islamabad, Pakistan**

**2021**

# DEDICATION

DEDICATED TO MY LOVING PARENTS WHO ALWAYS PRAYS FOR OUR SUCCESS AND OUR TEACHERS WHO ALWAYS INSPIRED US TO EXPLORE IDEAS OF LIFE WITH MODEST VISION AND FOSTER US THROUGH ODD AND EVEN SITUATIONS OF LIFE.

# ACKNOWLEDGEMENTS

With the blessing of all almighty Allah, the most charitable, forgiving and the creator of this beautiful world, today I am able to acknowledge after a fruitful completion of my research project. I also present my thanks in a modest and heartfelt way to the Prophet Muhammad (P.B.U.H) on behalf of which this universe exists. An inspirational messenger from Allah and great teacher who teach us the way of life and humanity.

It is my privilege to convey appreciation and to my research supervisor Dr. Iftikhar Hussain Gul and my GEC members Dr. Zakir Hussain and Dr. Sofia Javed for their constant help, advice, valuable comments, and efficient supervision at every stage of research work. Without their support, this work would not have completed.

I am forever indebted to my late father who taught me about values. His words of wisdom and prayers will forever be a source of encouragement for the rest of my life. May Allah bless his soul and make him stay in Jannat-ul-Firdous.

Last but not the least; A very special thanks to my beloved mother, brother, sister and friends for their encouragement and continuous support. I would also like to mention namely for their help whenever needed. I really do appreciate the support of my colleagues which proved to be a constant driving force for me to strive towards my goals.

Sincerely,

Muhammad Jahanzaib

# ABSTRACT

The exceptionally unique magnetic and electric properties of ferrites have always been of strong interest leading to their extensive commercial use. Barium hexaferrite, is one of the materials being used in microwave, electronic and magnetic devices. In present research study, cobalt and nickel substitution is performed in a series of $Ba_{1-2x}Ni_xCo_xFe_{12}O_{19}$ (x= 0, 0.1, 0.175, 0.25). Synthesis was performed using sol gel method and aqueous solutions of nitrates were used to prepare pure and doped barium hexaferrite nanoparticles. Calcination of the prepared samples was performed at 950 $^oC$ for 5 hours. The samples were characterized using Xray Diffraction, Fourier Transform Inferred Spectroscopy Vibrating Sample Magnetometer Scanning Electron Microscopy & UV Vis. Impedance analyzer was used to analyze the dielectric properties. Magnetic properties of the samples were studied using Vibrating Sample Magnetometer. XRD analysis confirms the hexagonal crystal structure of prepared $Ba_{1-2x}Ni_xCo_xFe_{12}O_{19}$. Crystallite size was calculated using Debye Scherer formula. Vibrating band positions were studied using FTIR. Dielectric studies revealed an increase in dielectric constant with the increasing dopant concentration. Similarly, with increasing x value, the dielectric loss value was also increased. Magnetic properties of the prepared samples showed an increase in magnetic saturation. A decrease in magnetic coercivity has been observed with increasing dopant concentration. The prepared samples showed an enhancement in dielectric and magnetic properties proving to be an efficient candidate for many magnetic and electrical applications. UV-Vis confirms the Photodegradation in the presence of Methyl-Blue the degradation process observed under the sunlight for 0-120mins at the rate of 30mins per sample concentration wise $Ba_{1-2x}Ni_xCo_xFe_{12}O_{19}$ (x= 0, 0.25).

# Table of Contents

# List of Figures

# LIST OF TABLES:

# Chapter 1

# Introduction Nanoscience and Metal Oxide Nanomaterials

# Introduction:

For any material to determine its properties it is way of construction matters and for construction, manipulation of matter can be done at any level, and this led to the development of a concept by Richard Feynman when he decided that physical laws cannot limit us to bulk material and as a result, he invented Nanotechnology. Nanotechnology is basically the study of manipulating materials at different levels including atomic, molecular, and macromolecular levels which results in the difference in their properties significantly at a large level. This technology allows us to control matter at a scale of $10^9$. Manipulating materials to a very small level makes it possible to introduce some new attributes which were not present in the bulk material and to explain the behavior and change in attributes of the materials at Nano level that differ from the bulk material quantum mechanics is to be applied. Now this technology is a part of every field including medicine, electronics, biosciences, physics, chemistry, robotics, pharmaceuticals, military, radar absorbing materials, photovoltaics, diagnosis and many other. The products made of nanotechnology are not only more reliable but also more efficient and cost effective. At nanoscale, the properties of materials change drastically. This is due to the large surface are and quantum confinement. Many semiconducting materials have change in their bandgap when in nano size. Band gap of silicon is reported to increase from 1.12 eV to 3.5 eV. Change in bandgap also provides change in semiconducting properties. Any material having at least one dimension less than 100 nm is classified as a nanomaterial. We can categorize nanomaterials as 0-dimensional, 1-dimensional, 2-dimensional, and 3dimensional on the basis of their dimensions.

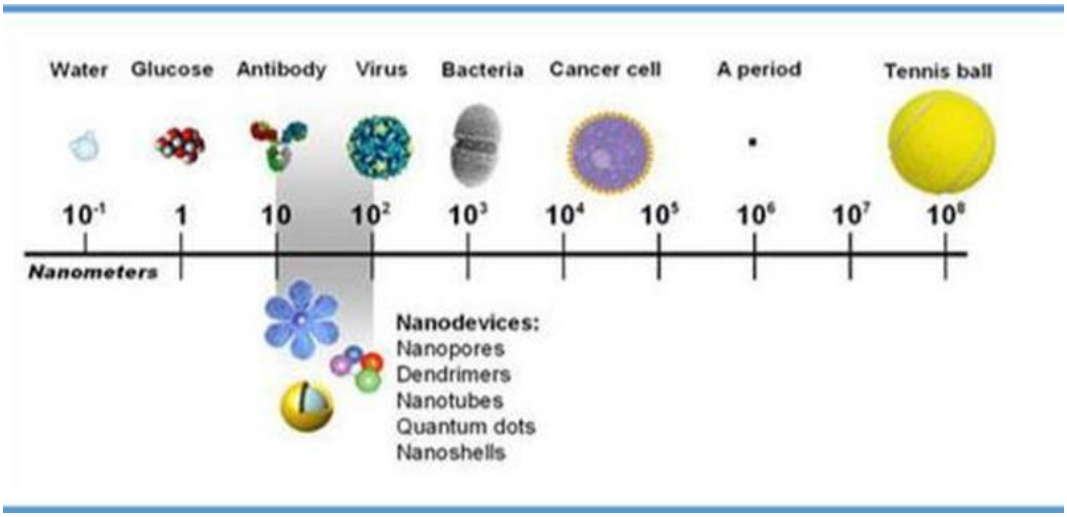


Figure 1.1: Macro to nano scales 1-100 nm [5].

## 1.1 Types of nanomaterials:

In nanoscience, entirely a new material has been synthesized instead of molding the previous ones' or by utilizing old techniques. The resultant materials have vital importance and have been applicable in multiple fields due to versatile properties these nanoparticles are carrying.

### 1.1.1 Zero Dimensional Nanomaterials:

0-dimensional Nanomaterials or quantum dots in which dimensions are measured within the nanoscale (1-100 nm). Confinement of holes and electron motion in these materials is in all directions. Nanoparticles, Nanoring's, Nanograins and buckyball ($C_{60}$) are the most common examples of 0-dimensional nanomaterials. These are also called quantum dots.

### 1.1.2 One Dimensional Nanomaterials:

These are the nanomaterials whose two dimensions lie within nanoscale while only one dimension lies outside the nanoscale. They have their applications in sensors, electronics, and optoelectronics due to their unique conducting and semiconducting properties. Most common examples of 1-dimensional nanomaterials include Nanotubes, Nano rods, and nanowires.

### 1.1.3 Two D Nanomaterials:

2-dimensional nanomaterials as the name indicate have 2 dimensions that lie outside the nanoscale. Most used 2-dimensional are the thin films which have various applications [1]. Graphene is also an example of 2-D nanomaterials with exceptional properties from electronics to drug delivery.

### 1.1.4 Three Dimensional Nanomaterials:

Nanomaterials with no dimensions confined to nanoscale and are bulk materials such as bulk powders, dispersion of nanoparticles and bundles of 1-D nanomaterials [1].

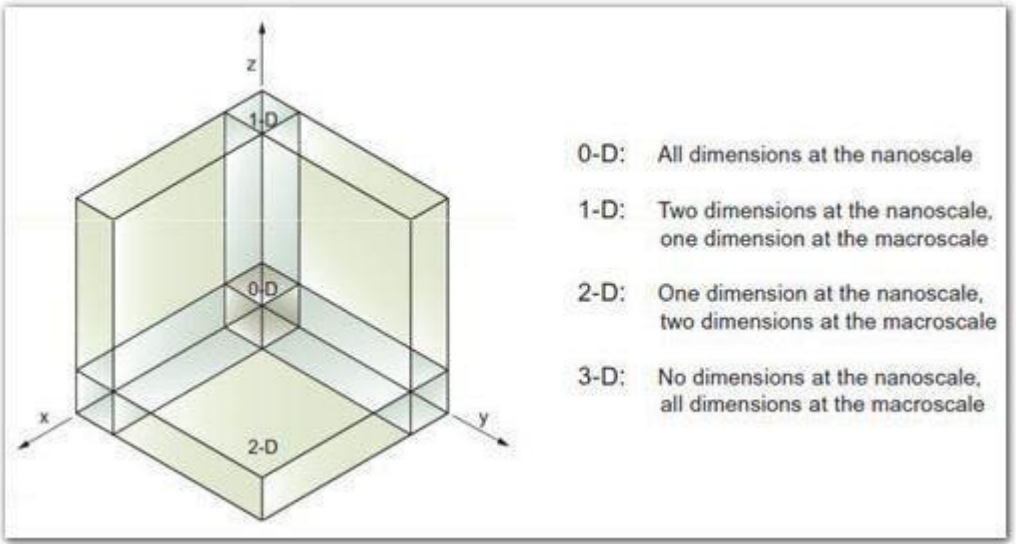


Figure 1.2: Classification of nanoscale dimensions

## 1.2 Magnetic Nanomaterials:

Magnetic nanomaterial is basically an area of research dealing with magnetic attributes of nanomaterials. They have been present in nature since beginning but discovered later [2]. Due to the presence of magnetic nanoparticles in insects and bacteria their discovery become quite easier. Versatile applications of magnetic nanoparticles make it a major field to study in last few years. Characterization of synthesized magnetic materials have been favored by new advancements in technology [1]. Their synthesis can be made possible in various shapes like spheres, rods, fibers, and polyhedrons and in different forms like as particles or

even nanowires, mono or multi layered films, dispersions, and agglomerates but the major focused is on the synthesis of magnetic nanoparticles [4]. Materials having transition metals in them have gained much importance among all nanomaterials. These materials include iron, cobalt, nickel, and their alloys.

Ferrites either Pure or mixed, have unique properties which makes them able to gain special attention. Because of easy synthesis and stability in aqueous medium synthesis of nanoparticles ranging from as less as 1-10 nm can be possible. Quantum size makes effect and change in the surface area of the magnetic nanoparticles and thus several nanoparticles start to have a super paramagnetic phenomenon and quantum tunneling, and this makes it possible for the magnetic nanoparticle to behave as a single magnetic domain [6]. Magnetic substances can be classified based on the applied outside field along with the responses of these substances to that applied field. Magnetism have been classified into 5 basic types. These are named as diamagnetism, paramagnetism, ferromagnetism, ferrimagnetism, and anti-ferromagnetism.

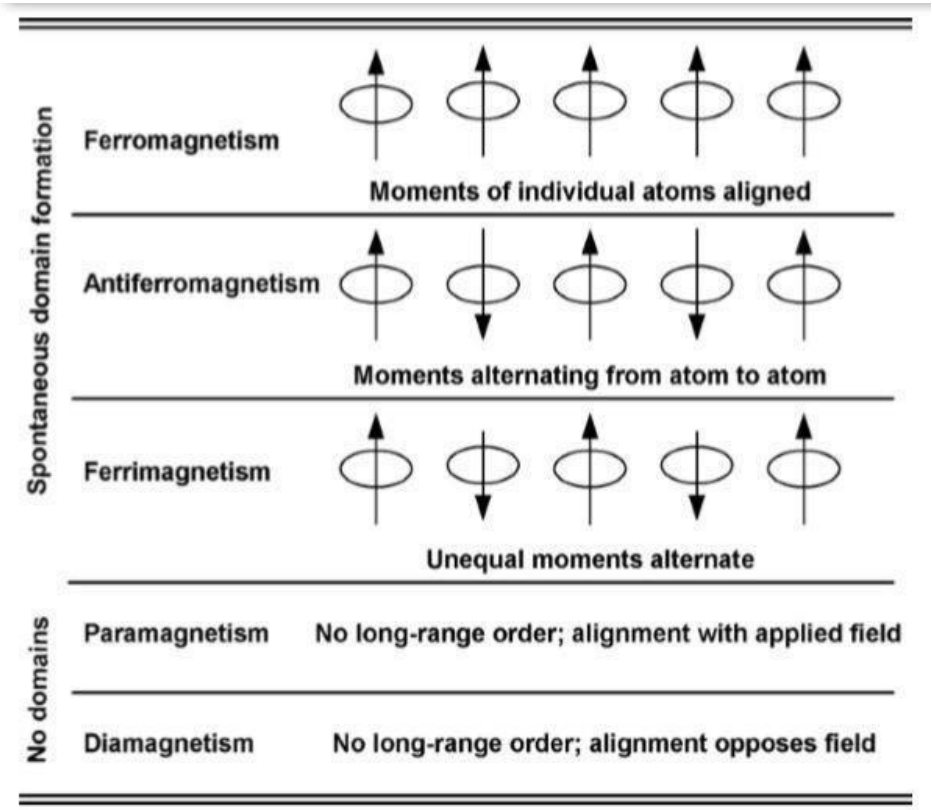


Figure.1. 3: Classification of nanoscale dimensions regarding magnetism

### 1.2.1 Ferrites:

Ferrite is a ceramic material which is composed of iron and oxygen with a composition of 2:3, respectively. Composition of ferrites includes iron oxide along with other metallic elements or oxide materials having ferric ion i.e., $Fe^{+3}$ as a main constituent. Magnetic property of Ferrites depends on their magnetic ion as ferrites is ionic compounds. They are brittle in nature and their color is darkish color and they possess polycrystalline properties [7]. Ferrites contain ferromagnetic oxides that give them ferromagnetic properties and contain metal oxides along with ferric oxides [6]. Ferrites have different magnetic moments such as parallel or perpendicular moments enabling them to have exceptional magnetic properties and unique crystal structure. Exceptional and diverse arrangement of ferrites make them different from other nanomaterials and hence they have varied range of applications [6]. Spinel ferrite among ferrites are the nanoparticles that have gained a huge interest in determining major magnetic properties that are the basics of science. These ferrites have also enabled us to determine the relationship between the crystal structure and magnetic properties. It is the chemistry of the crystal that explains the internal structure along with the physical attributes of a material thus helps in understanding the link between them [5]. Because of their magnetic and electrical properties spinel ferrites gain importance worldwide and being studied on global level and are applicable in varied fields such as medical devices, storage, magnetic fluids, microwave absorbers etc.

Moreover, they have a very high electrical resistivity which helps them in gaining the ability to limit the generation of eddy currents thus results in the reduction eddy current loss. Beside resistivity, ferrites also have a value of permittivity, permeability, ability to saturate, magnetization but exposure to high temperature can cause major decline in magnetization properties.

In the last few years' ferrites gain much importance and super paramagnetic metal oxide nanoparticles acquire attention to be prepared and characterized. Tunneling of electrons and super paramagnetic properties of a material can easily be explained by understanding the crystal structure of ferrite nanoparticles [9].

With these above-mentioned wide range of properties and ability to have different properties with varying mixture of iron oxide and other materials gives us opportunity to tailor and get electrical and magnetic properties according to our desire and need. Magnetic North has been located first time in the history using magnetic iron oxide.

### 1.2.2 History of Ferrites:

To mankind Ferrites are not Nobel but they are new in the field of science. Knowledge of manipulating or synthesizing ferrites have been not known to people till centuries however they have using them in their daily life to make it easier [9]. But with the passage of time, they have gained the knowledge, gain the abilities and properties to work with these materials. “Ferrite” was derived from Latin language word “ferrum” means “Iron” while iron being important component of ferrites or simply magnetic oxides. Explanation of an ancient known ferrites found in about 800 B.C Greek history is “loadstone” also called magnetite ($Fe_3O_4$) is a naturally occurring nonmetallic solid and attracts iron also. Term Magnetism was also familiar to ancient people [9]. Among ancient people Chinese were familiar with the properties of loadstone and they had even utilized it in compasses for navigation purposes to locate magnetic North of earth. Use of magnetic iron oxide loadstone for the first time in the history to locate magnetic north made it clear to the people that Earth itself is a magnetic in nature [7]. These all research were made in $17^{th}$ century. Also, in 1600 physicist William Gilbert has first ever published a scientific study on magnetism called “De Magnate”. Another scientist Christian Oersted in 1819 noticed the deflection in needle of magnetic compass when brought near to the electric current carrying wire which led to the discovery of electromagnets in 1825 [5]. Practically the use of ferrites and their applications were started in1930 while keeping in consideration the properties like physical, magnetic, and electrical properties researcher started their huge study on them.

### 1.2.3 Ferrite Structure:

Keeping specific example of spinel ferrites structure of ferrites are to be discussed which have a cubic closed packed structure having formula $MeFe_2O_4$ where Me is the metallic ion. Me and Fe are at the two different crystallographic sites and at

these sites' coordination of tetrahedral and octahedral sites of oxygen can be found and the final local symmetries are different for both mentioned sites [2]. These sites can be defined as A and B sites with A sites being 8 and B sites being 16. A site possesses tetrahedral coordination of the metallic ion with oxygen and b sites possess octahedral coordination of the Fe ion with oxygen. When metallic cations possess the A sites and Fe cations possess the B sites then the ferrite is known as a normal spinel ferrite [1]. If the Fe cations possess the A sites completely and the B sites are randomly occupied by Me and Fe cations, then the ferrite is known as an inverse spinel ferrite. Magnetically ferromagnetic ordering is displayed by spinel ferrites. Magnetic moments of cations align parallel with each other.

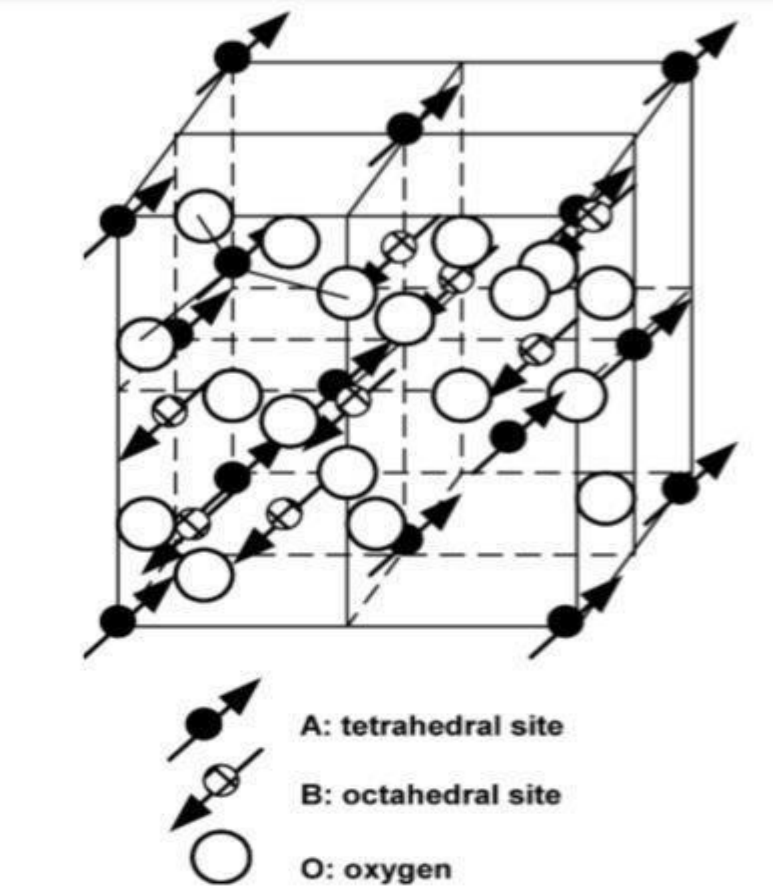


Figure 1.4: A partial unit cell & spinel ferrite structure in ferromagnetic ordering

### 1.2.4 Ferrites Types:

Based on hysteresis loss, structure and behavior ferrites have been classified. Based on magnetic behavior or hysteresis loss ferrites have been classified as:

- Soft ferrites
- Hard ferrites [3]

While based on structure ferrites are classified as:

- Spinel ferrites
- Garnets
- Hexagonal ferrites

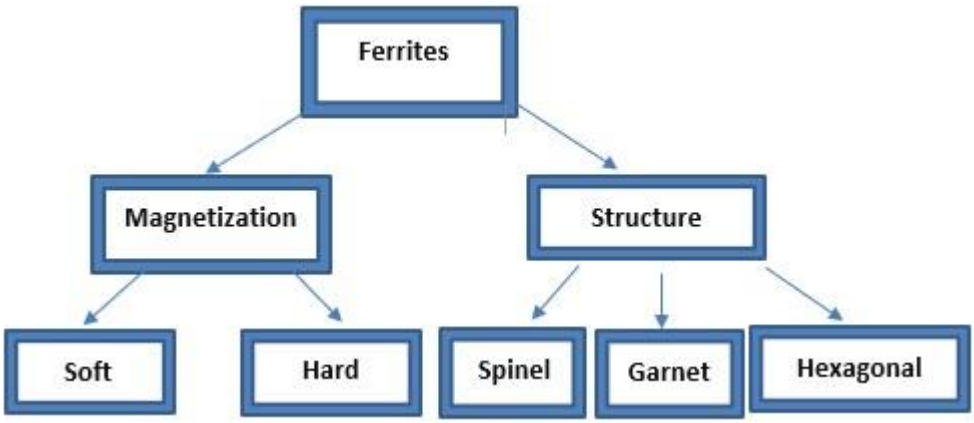


Figure 1.5: Classification of ferrites.

### 1.2.5 Soft Ferrites:

Soft ferrites have very low energy dissipation in magnetization and de magnetization along with low coercivity [2] because when a magnetic field is present, they magnetize and de magnetize very easily. Soft ferrites have low permeability and low coercivity and their coercivity is always less than 1000 A/m and they are also having narrow hysteresis loop that's why low saturation magnetization, low magnetostriction and low Curie temperature [3]. They must bear high resistivity values. Energy losses in transformer cores and inductors have been prevented by them. Their further characteristics include their different color range appear from dark black to gray and they have been very hard and brittle. These ferrites have multiple applications including small size antennas, power

electronics circuits, chocks, inductors, volatile and nonvolatile memories. Most common examples of ferrites are $MnZnFe_2O_4$ and $NiZnFe_2O_4$ etc.

### 1.2.6 Hard Ferrites:

Those ferrites which have wide hysteresis loop and on the presence of magnetic field they do not magnetize or demagnetize in-fact take more time for magnetization are call as hard disk [10]. They have certain exceptional properties which makes them to be a permanent magnet including high value of coercivity, high remanence, high saturation magnetization, high magnetostriction, high permeability along with high Curie temperature (Tc) [2]. They can easily be synthesized as raw materials required for their synthesis are easily available, thus they are not costly. This property makes their use on daily basis even in household appliances, cars, electrical devices. They can also be used as a purpose of high-density storage and in audio and video tapes. $BaFe_{12}O_{19}$, $SrFe_{12}O_{19}$ and $CoFe_2O_4$ are the most common examples of hard ferrites. These applications of hard and soft ferrites and their low costs make ferrites very useful candidate in the innovative applications [3].

Table 1.1: Comparison between Soft and Hard Ferrite

| **Comparison** | **Hard Ferrite** | | **Soft ferrite** | |
|---|---|---|---|---|
| | **High** | **Low** | **High** | **Low** |
| **Saturation Magnetization** | | ✔ | | ✔ |
| **Coercivity (Hc)** | ✔ | | | ✔ |
| **Permeability** | | ✔ | | ✔ |
| **Remanence** | ✔ | | | ✔ |
| **Magnetostriction** | ✔ | | | ✔ |

### 1.2.7 Spinel Ferrites:

Spinel ferrites are considered as the subtypes of Cubic Ferrites. In 1915 Braggs and Nishikawa have first discovered the structure for the spinal ferrites also termed as spinal structure.

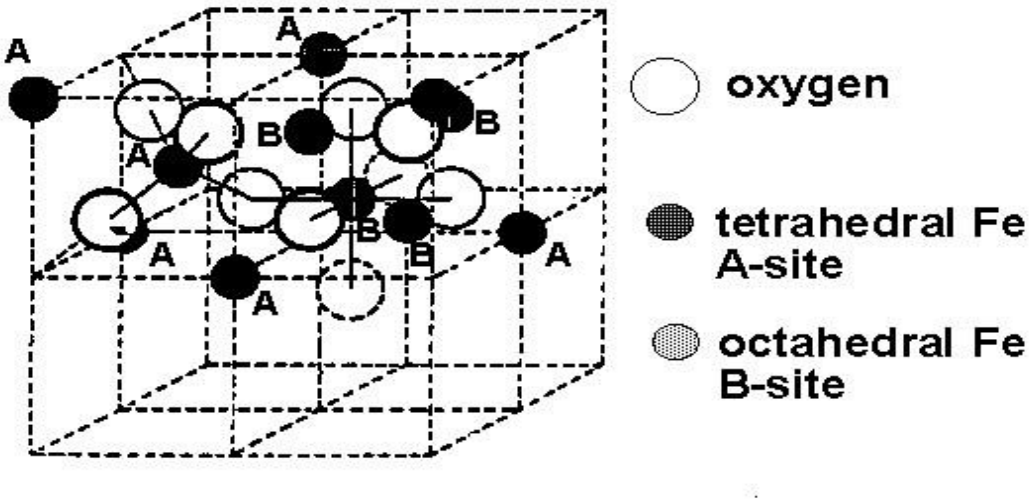


Figure 1.6: Spinel ferrite unit cell with octahedral and tetrahedral site [6]

Their structure has two sites, one is Tetrahedral which is denoted by A and the other is Octahedral denoted by B as mentioned in fig 1.2. A site has been surrounded by 4 oxygen atoms while B site has been surrounded by 6 oxygen atoms [7]. 32 Octahedral sites in total are found in spinel ferrite structure and among them 16 are surrounded by anions. Presence of these two exactly different sites makes the entire structure electrically neutral and they rarely have magnetic and electrical behavior [6]. On the basis of their cations dispersion in tetrahedral and octahedral is further classification of these ferrites have been made. [7].

They have been classified in the following groups.

- Normal Spinal Ferrites
- Inverse Spinal Ferrites
- Mixed Spinal Ferrites

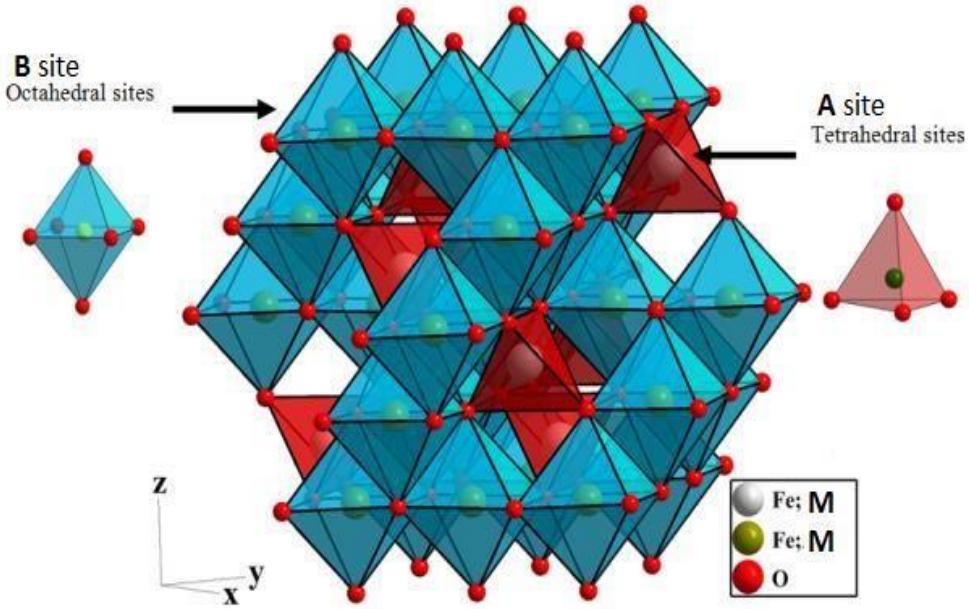


Figure 1.7: 3D model of Octahedral and tetrahedral sites in unit cell [8]

For better and detailed understanding of ferrites spinel ferrites have been discussed thoroughly in this chapter which give us with more insight about ferrites and to make things clearer and to broaden the knowledge about ferrites, brief discussion of abovementioned types of spinel ferrites is as follows:

#### 1.2.7.1 Normal Spinel Ferrite:

As now it become clear that ferrites are composed of divalent and trivalent metal ions so the spinel ferrites whose B sites are being held by a trivalent metal ion within a crystal structure while on the other hand A sites which are tetrahedral are held by divalent metal ions are called normal spinel ferrites.

#### 1.2.7.2 Inverse Ferrites:

Spinel ferrites in which within crystal structure both sites A (tetrahedral) and B (octahedral) are partially occupied by trivalent metal ions while remaining divalent metal ions are being distributed on B sites only are called inverse spinel ferrites [7].

#### 1.2.7.3 Mixed Ferrites:

Mixed Spinel Ferrites" are the third form, In these ferrites both sites A and B are occupied by both trivalent and divalent ions. In mixed spinel ferrites unlike

inverse spinal ferrites number of trivalent and divalent ions on octahedral sites are not equal [7].

Table 1.2: Types of spinel ferrites, Summary

| **Types of spinel structures** | |
|---|---|
| **Normal spinel** | "**A site**" contained by metal cations while "**B site**" by $Fe^{3+}$ cations. |
| **Inverse spinel** | $Fe^{3+}$ cations completely occupied **A site** and **B site** randomly by both Metal cation and $Fe^{3+.}$ |
| **Mixed spinel** | Both **A** and **B** sites occupied by cations intermediately. |

### 1.2.8 Garnet Ferrites:

In 1957 Giller and Gilleo discovered the garnet ferrites. Garnet ferrites have a molecular formula $M_3 Fe_5O_{12}$ where M is the rare-earth trivalent ions. Rare earth metals examples also include Gd, Dy and Y ions. Their structure is cubic, and they have magnetically hard nature. [3]

### 1.2.9 Hexagonal Ferrites:

Hexagonal ferrite has a general formula $MFe_{12}O_{19}$ where M can be barium, cobalt Barium, or combo of all these elements. There is a structure similarity between hexagonal ferrites and spinel ferrites. Octahedral, tetrahedral, and trigonal are the three sites in these ferrites in which metal ions are being occupied. There are two types of layers of oxygen in their hexagonal structure. Each layer has a different composition of oxygen ions for example, there are four oxygen ions in the first layer while there are three oxygen ions in the third layer and in the second layer the site which is devoid of oxygen is occupied by barium ion [3]. Along with the two oxygen layers tetrahedral, octahedral, and trigonal bipyramidal interstitial sites are also present in these ferrites which are found between the layers

surrounded by four, six and 5O ions respectively [8]. Their practical application is due to their immense range of coercivity. Moreover, these materials are significant in the field of electronics and telecommunications. They have their wide usage in loudspeakers, microwave applications, magnetic recording devices and as fridge magnets [5].

## 1.3 Cobalt (Co) Ferrites:

Cobalt ferrite is a type of ferrites that has immense importance thus gain a lot of attention of the researchers due to its great applications in magnetic fluids, magnetic recording devices, high resistivity, and many others [5]. They have a general formula $CoFe_2O_4$. Cobalt ferrites have a great chemical stability and excellent mechanical hardness. Cobalt ferrites are the cubic ferrites and have the inverse spinel structure and as mentioned earlier A and B sites has $Fe^{3+}$ located on them while $Co^{2+}$ is located only at B site [4]. This ferrite has the anisotropy constant value in the range from 1.8 to 3 x $10^6$ erg/$cm^3$. High value of coercivity makes the use of these ferrites in the magnetic recording devices and this high value of coercivity is determined on the basis on the size of particle of the material. For the preparation of these ferrite Nano-particles synthetic methods used are the Sol gel and Co-precipitation methods. [9]. Fe-III and Fe-II salts are also used for the synthesis of the cobalt ferrite nanoparticles. Cobalt ferrites have properties like electrical and dielectric properties are of great importance and because of these properties' cobalt ferrite has many applications. Size of the grains and crystal structure of these ferrites are the characteristics which makes factors like dielectric constant, dielectric loss, ac and dc electrical resistivity dependent on them [11].

## 1.4 Silver (Ag) :

Silver is a metal which has been the part of ferrite composition to some extent have immense importance since the history of mankind. It has great benefits and is advantageous right from the early times. Its usefulness is attributed to its easy availability and its presence in uncombined form, and it were easily mined out of it in central and south America, Peru, Germany. It has some unique characteristics like soft and shiny metallic look. Due to the presence of Sulphur in atmosphere it tarnishes very quickly in air as it is reactive to sulfur. One of the most common

and interesting use of silver is as currency from ancient times back to Romans and Greeks. People use it as a currency by mixing it with or both of them separately. One more interesting use of silver is in Jewelry because of silver being good conductor of electricity. Its conductivity is even higher than the copper which also makes it useful for electronic or electrical purposes for creating electrical contacts. The paint of the silver is utilized in producing printed circuit boards. It is actually the properties of silver that makes it capable of being used for different purposes such as its property of high reflection it is used to make mirror and find great application in the field of physical Optics. Moreover, it is used in photography, in light sensitive glass of lenses as it is sensitive to visible light. Bearing great antibacterial properties, it has its role in medical industry. It also has its applications in electronics industry and used in clothing against bacteria.

## 1.5 Ferrites and their Electrical Properties:

Materials are basically categorized into three basic classes. Conductors, semiconductors, or insulators on the basis of their ability to deal with the electricity they can allow to flow through them or their ability to carry electrical charges [2]. Those materials which are excellent carrier of electrical charges or can allow electricity to flow through them are conductors and these materials have lower activation energy. On the other hand, insulators do not allow electric current to flow through them or are not the carriers of electric charges thus they have very high activation energy. By increasing temperature of some insulators and semiconductors their conductivity increases but in case of metals with increase in temperature a gradual decrease occurs in their conductivity.

Ferrites are structure sensitive materials and the flow or conduction of electric charges in the ferrites depends on the structure of these ferrites. To change the behavior of ferrites their structure can be modified by its synthesis route, number of substituents, annealing temperature, reaction temperature and by the type of substituents [2]. By controlling these factors electrical resistance of ferrites can be controlled and enhanced and in comparison, to metals, ferrites contain a high value electric resistivity. [19]. According to the Verwey Model conduction or transport of charge carriers occur in the form of hopping in ferrites which occurs between the ions at octahedral sites.

There must be high energy possessed by the charge carriers so that they can easily jump from one ion to another which result in active electrical conduction in ferrites because charge carrier must have high potential to over the barrier for jumping between the ions. Minimum energy possessed by the charge carrier in order to overcome the potential barriers is called activation energy [21]. The transportation of charge carriers in M-type ferrite materials is also occurred by hopping thus they are hopping semiconductors as these materials have large number of mobile electrons [22]. The hopping mechanism of electrons ferrites occurs in between the di and trivalent iron ions which are situated at the octahedral sites [21]. This exchange can be different in different materials depending upon the orbital overlapping of $Fe^{3+}$ and $Fe^{2+}$ with oxygen [23].

## 1.6 Dielectric Properties of Ferrites:

High resistivity of ferrites at room temperature indicates that ferrites have high activation energy, and this is the specific property which makes ferrites them suitable for their applications as dielectric materials. Mainly the materials used as dielectric are the nonconducting materials. To study the interaction of electric field with the atoms of dielectric materials is very important and informative as well. Polarization in the dielectric materials only occurs when they are put into an electric field, and this happens because of the occurrence of induced dipole moments. When a field is given to the electron, cloud move to one side resulting in the creation of dipoles which is characterized by its dipole moments. Atoms of the dielectric material creates their own small field which interact with the field which is applied from the outside. Negative charged electron cloud and positive ions of atoms are separated from each other and thus the dipoles are oriented accordingly to the field that is applied from the outside. This separation or detachment of charge carriers at the grain-boundaries due to the electrical field is known as electrical polarization.

Interfacial polarization or space-charge polarization is the reason of electrical polarization because of its linkage with the charges being trapped or mobile. Amorphous and polycrystalline materials have this type of electrical polarization as these materials have charge carriers like electrons, holes and ions are trapped on some sites and they get mobilize after getting some energy [16]. Dielectric

behavior of any material is greatly dependent on the nature of material or a substance and dielectric constant of a dielectric material mainly dependent on the following factors:

- Frequency of changing electric field.
- Rate of change of time-varying field.
- Chemical structure of dielectric material.
- Imperfection (defects) of the material.
- Physical parameters like pressure temperature.

Dielectric polarization and its constant both are dependent on each other. External field fluctuation results in the fluctuation of dielectric polarization and if dielectric polarization fluctuations do not complement with the fluctuations in external field, then there must be a decrease in dielectric constant of that material [17]. Dielectric constant would remain the same if the external field applied has low frequency value because it causes fluctuation follows by the dielectric constant polarization to remain low as of external field but if the frequency applied by the external field is high then the polarization will not be able to follow the field and its dielectric constant decreases and then a stage comes when the polarization stops due to relaxation of dielectric materials [18]. There are different limits of frequencies at which the different types of polarization (ionic, electronic etc.) stops.

## 1.7 Magnetism:

To understand magnetic behavior of ferrites thorough understanding of magnetism is given discussed. The history of magnetism is very old, but its understanding began in $20^{th}$ century. Chinese is the ancient nation who had used magnets in various navigation applications such as compass in the 12 centuries. William Gilbert a physicist manufactured some artificial magnets and showed that the compass will point towards North-South because Earth itself has a magnetic property. John Michel in the $17^{th}$ century, showed that this inverse square law that is followed by the magnetic poles and the same concept was later proved by

Charles Coulomb. The first electromagnet was manufactured in 1825 when the fact was discovered that magnetic field is produced by an electric current. Faraday, Becquerel, and Bergmann later discussed the effect of magnetism on liquids and gases and found out some of them has a noticeable extent. The whole idea of magnetism floats around the magnetic field and the dipoles. The magnetic field is basically the area or space in which changes in the energy occur and his change can be detected and measured easily while the magnetic poles describe the area of magnetic field. Magnetic poles occur in two opposite poles rather than in isolation. Magnetic field entering the dipole is described by the South pole while the North pole describes that the magnetic field is leaving the dipole. By cutting the magnet bar into pieces, two or more dipoles or magnets can be created.

Each material's response to magnetic field is different as some got attracted while some got repelled by the magnetic field and some remain unaffected when they are subjected to the magnetic field. But the response to magnetic field gets vanished on a critical temperature which was studied by Curie; he examined that magnetic materials response no magnetic behavior after a certain temperature which is termed as Curie temperature. Every material has its own Curie temperature for which it shows no magnetic response.

To understand the concept of magnetism some basics concepts are to be cleared first. Knowledge of atoms and matter is the initial knowledge which is explained as anything which has weight and occupy some space is called matter and matter is composed of atoms. Further knowledge revealed that atoms also have constituent's particles. It consists of protons, electrons and neutrons and protons and electrons are the sub-atomic particles that carry charges. Protons carry positive charge while electrons are negatively charged particles while neutron being neutral. Proton and neutron exist inside atom's nucleus while electrons revolve around the nucleus along with its own axis having constant motion and revolve round its own axis. This movement of electron around nucleus creates magnetic field due to the charge in movement [24]. Movement of electrons around its own axis is same as the Earth's rotation around its axis. Motion of an electrical charge creates magnetic field. According to Pauli Exclusion's Principle if there is a large fraction of elements the magnetic moment of electrons will cancel each

other and Pauli's electrical charge which is in motion creating a magnetic field of opposite spin can be present in each electronic orbit. There are few transition metals that do not cancel magnetic moment i.e., Fe, Ni and Co; and these are the ideal examples of magnetic materials. From the spin of electrons in these transition metals magnetic moment arises. Europium, neodymium, samarium, and cerium are the rare earth metals that shows magnetic behavior and do not cancel the orbital motion of electrons [2]. Some chemical compounds also show magnetism due the presence of rare earth metals and transition metals and example of these compounds include metal oxides where oxygen is bonded with metals.

### 1.7.1 Types of Magnetism:

Material on placing in a magnetic field shows varied types of behaviors and this all depend on factors such as the net magnetic moments of atoms or the atomic and molecular level of structures. By applying external field magnetic moment which is associated with the motion of electrons can be altered and on application of external field materials have different response such that some align themselves to the field while other align themselves opposite to the field. Magnetic field got cancelled as electrons are usually found in pairs in an atom which spin in opposite directions [2]. Materials having unpaired electrons show some net magnetic field. Based on these characteristics, the magnetic behavior can be classified as follows,

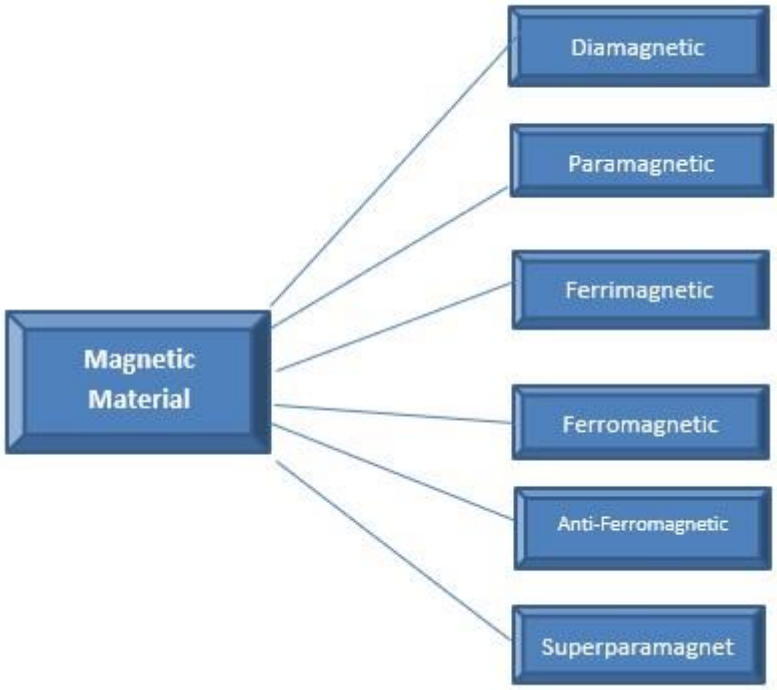


Figure 1.8: Types of magnetic materials

### 1.7.2 Diamagnetism:

If in a magnetic material magnetic moment is zero, then there would not any internal magnetic interactions are called diamagnetic materials. These are the materials whose external shells are completely occupied by the atoms. The change in orbital angular momentum induces a magnetic moment in the diamagnetic material is induced by the change in angular momentum of the orbital. These materials always oppose the external applied magnetic field thus they have a negative susceptibility. Elements like $N_2$, He, $H_2$ and compounds like NaCl have diamagnetic properties because these are the materials which have filled outermost shells [2].

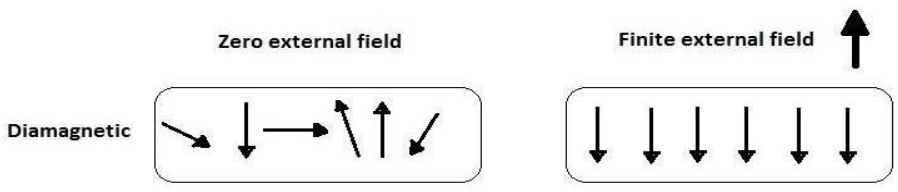


Figure 1.9: Atomic dipole configuration of diamagnetic material [7]

### 1.7.3 Paramagnetism:

Materials which show magnetization only in case when external magnetic field is applied are called paramagnetic materials and the phenomenon is called paramagnetism. Paramagnetic materials consist of permanent dipoles and these dipoles are randomly oriented inside the magnetic materials when they are not exposed to the external magnetic field. Dipoles are arranged in such a way that they are unsymmetrical to each other thus canceling the magnetic effect of each other and as a result there is (zero) 0 net magnetic effect on the material. On placing paramagnetic substance in an external field, a torque is provided to the magnetic dipoles and as a result they align themselves in a proper direction thus get magnetized but magnetic properties get vanished when externally applied magnetic field is disconnected as it causes alignment of dipoles to go back to their original position and causes loss their energy. In comparison to diamagnetic material, paramagnetic materials show positive susceptibility as they are attracted to the source which applied an external magnetic field while diamagnetic materials show negative susceptibility.

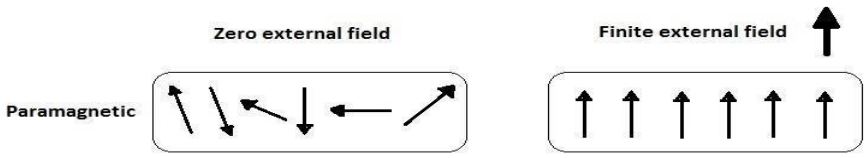


Figure 1.10: Para magnetic material Atomic dipole configuration [7]

### 1.7.4 Ferromagnetism:

Ferro magnets are also the magnetic materials that show magnetization in the lack of an outer magnetic field called ferromagnetism. They also show similarity to paramagnetic materials as ferromagnetic materials show positive response and get attracted by external fields. On placing ferromagnetic material under curie temperature in the external magnetic field by giving, the atomic magnetic moment of all atoms aligns exactly to the direction of applied exterior field but on the removal of external magnetic field ferromagnetic material shows magnetization

again even in the nonexistence of exterior field. Materials ferromagnetic properties changes to paramagnetic material when there is an increase in the curie temperature. Although even in the existence of weak external magnetic field ferromagnetic material has high saturation magnetization due to rapid increase in magnetization. Fe, Co, Ni, Sr and Br are the elements that show ferromagnetic nature [2].

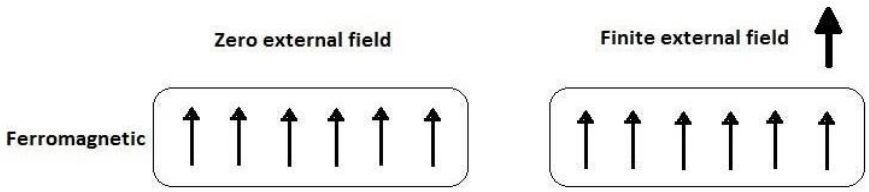


Figure 1.11: Ferromagnetic material Atomic dipole configuration [7]

### 1.7.5 Ferrimagnetism:

In case of ferromagnetic materials magnetic moments of linked atoms is oppose in direction but not equal in magnitude but in case of antiferromagnetic materials magnetic moments are opposite and equal in magnitude. Under curie temperature, ferrimagnetic materials hold spontaneous magnetization which got vanished on an increase in temperature from curie temperature and have no magnetic order [5].

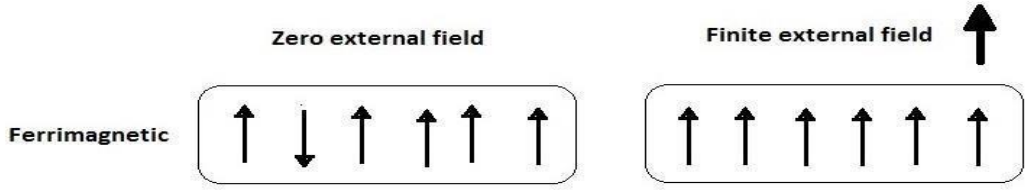


Figure 1.12: Ferrimagnetic material Atomic dipole configuration [7]

### 1.7.6 Anti-Ferromagnetism:

Anti-ferromagnetism occurs when there is an antiparallel arrangement between the spin of electrons of the neighboring atoms [4]. Under anti-ferromagnetic behavior a crystal consists of two lattices among which one is magnetized in opposite direction to the second lattice. This behavior was observed in 1938 in MnO. There is no clear magnetization in the lack of exterior magnetic field because atoms cancel the effect of each other but when the exterior field is applied dipoles align in the direction of the given magnetic field and show small net magnetization which will increase with the increase in temperature until a critical temperature called Neel temperature. This behavior only exists at low temperature and vanishes at the temperature above the Neel temperature. MnO, NiO, Cr, FeO and CoO are the ideal examples of Anti-ferromagnetic materials.

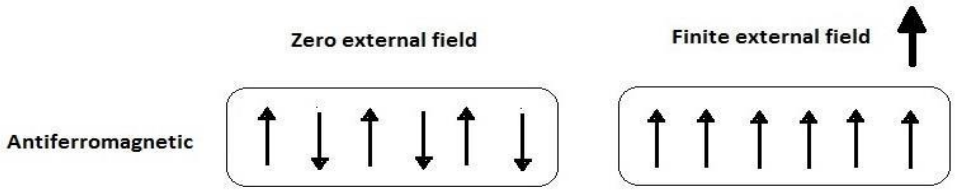


Figure 1.13: Antiferromagnetic material Atomic dipole configuration [7]

### 1.7.7 Super Paramagnetic:

When the material shows a paramagnetic property under the Curie temperature or Neel temperature the resultant phenomenon is called super-paramagnetic, and the materials are called super paramagnetic materials. Resultant temperature when a ferro-magnetic or ferri-magnetic behavior is converted into paramagnetic behavior is called Curie temperature. In these materials, the coupling force causes the magnetic moment of adjacent atoms to align and results in a large internal magnetic field. The magnetic susceptibility of converted paramagnetic behavior is much larger than that of paramagnets.

## 1.8 Application of Ferrites:

High resistive value makes ferrite a vital magnetic material. At high frequencies, ferrites have many applications. They have various characteristic properties such as high DC electrical resistivity, coercivity, stiffness, good magnetic properties, and low eddy current loss. They are cheap also and have wide selection of materials. They are chemically stable over wide range of temperatures. All these diverse properties of ferrites make them to be applicable in many fields such as recording tapes, magnetic equipment, permanent magnets, switching devices, color imaging, flexible recording media and hard disc recording media. They are also used to make transformer cores, permanent magnets and in other so many applications [3]. Some of ferrite's applications can be in Microwave devices, Drug delivery, Data storage, Electromagnetic absorbers, Core material & Ferrofluids etc

# Chapter No. 2

# Literature Study:

In this chapter, literature survey on the subject is carried out systematically. Hexaferrites of different compositions have been studied since long and used in many practical applications. Due to the extensive research on ferrites, it is not possible to gather important data and results about the entire work done.

The given literature is only restricted to the systematic review of different theoretical and experimental facts related to present study including Ni-Co based Barium hexaferrites.

## 2.1 Barium based Hexaferrites (BaM):

### 2.1.1 Short History of BaM:

Prominent advancements in magnetic materials rare earths, such as Yttrium Cobalt ($YCo^5$) starts in 1960 and the years that followed makes the use of rare-earth (RE) and a Transition Metal (TM). RE&TM combo gives an ideal one composition as anisotropy has been provided by RE element while TM material gives maximum magnetization with huge power product and high-level Curie temperature. Following this, Samarium Cobalt has been discovered in 1967 and it is referred to as first commercial RE/TM long-lasting magnetic material. Different forms of ferrites specially soft ferrites were then developed later on along with paper publishing work on ferrites has been done in 2011.

Various research has been carried to develop hexaferrites using number of techniques and their features. Extensive work on the other hand, has been done to find the effect of various dopants for Ba and Fe in M-type barium hexaferrites (BaM).

It was found that doping of rare earth ions in BaM material substantially affects their properties.

### 2.1.2 Literature survey for M-type Barium hexaferrites:

Work carried out in past few years on different processing methods and using different dopant ions is given below:

Barium Hexa-ferrites ($BaFe_{12}O_{19}$) were prepared by *Radwan et al* with the help of coprecipitation-calcination process. In the process they used barium and ferric chloride as their initial precursor and then by the use of hydroxide solution they precipitate the barium and iron ions. The pH value of the solution was 10 at room temperature. The calcination temperature for the calcination of the precursors was 800-1200$^{o}$C for 2h. The magnetic properties of the produced ferrites particles were studied. They found that the number of formations of single-phase $BaFe_{12}O_{19}$ nanoparticles increases as they increase the calcination temperature. One can also achieve the uni-phase $BaFe_{12}O_{19}$ powered by the help of decreasing the mole ratio$Fe^{3+/}Ba^{2+.}$

In 2000 *Gonzalez-Carreno T.*et al worked by the combination of two techniques on the nanoparticles of $BaFe_{12}O_{19}$ (10 nm in diameter), the citrate precursor and the aerosol pyrolysis [35]. After the heat treatment, the hexaferrite phase was found at 1000$^{o}$C while particle size reaches to 100 nm in diameter. Saturation magnetization and coercivity values obtained for the largest particles were in comparison with commercial values, 50emu/g and 5600 Oe (kA/m), respectively.

In 2000 *Ng WK, Ding J, Chow YY, Wang S, Shi Y* used chemical Co-precipitation method [36] for the preparation of delicate fragments of barium ferrite with high coercivity (450kA/m). Barium ferrite's magnetic properties were determined at different temperatures and Ultrafine dispersed barium ferrite particles were obtained by mechanical milling. Remanence and weak anisotropy in the coercivity stemmed in the directions parallel and perpendicular to the compaction direction.

*Roberto Da Costa Lima et al.* in 2004 studied the "Effect of double substituted m-barium hexaferrites on microwave absorption properties". In polychloroprene (CR) matrices, they investigated the real and imaginary components along with their connection with microwave absorbing properties in the frequency range 8-16 GHz for doped M-type barium hexaferrites. By the addition of dopants, it was

found that the reduction in the coercive field and magnetization of barium hexaferrites has been resulted. Dual substitution of $Ba^{2+}$ and $Fe^{3+,}$ which occurs in the composite at the ratio of 80:20 of LaNaCo-TiMnBa to Cr, produces a better RAM at 15 GHz, as compared to individual substitutions, with the reflection loss of -30 dB (microwave absorption of about 99.9%).

*Sunil Kumar et al*. had synthesized chromium doped barium Hexa-ferrite using modified sol-gel method. Various concentrations of chromium were used to evaluate the effect of doping on various properties. XRD results confirmed single phase nanocrystalline structure with no impurity phase. Magnetic hysteresis loop was obtained using Law approach to saturation method, revealing the ferromagnetic nature. Magnetic coercivity and anisotropy seemed to increase as the chromium concentration increases.

In 2007 *M. Radwan et al.* worked on barium hexaferrite nanoparticles by chemical coprecipitation. The effect of Fe/Ba molar ratios were studied, and samples were calcined at different temperature. The formation of single-phase barium hexaferrite was increased by the addition of surfactants at low calcination temperature and very helpful in controlling microstructure.

*Hamid S. Al-Jumaili* in 2007 studied the effect of Mn and Ti substituted barium ferrite on the electromagnetic microwave absorber in the X-band range. For the X-band frequency range (8-12GHz), the frequency dependence of reflection loss (R.L) obtained a minimum value of -21dB and gives a band thickness more than 1GHz in the similar frequency span. The grain size obtained for the prepared powder was between (7.05-12.06 um) [31].

*Hsing-I Hsiang & Ren-Qian Yao* in 2007 studied "Hexagonal ferrite powder synthesis by chemical coprecipitation. The formation mechanism of $3BaO.2CoO.12Fe_2O_3$ ($Co_2Z$), $2BaO.2CoO.\ 6Fe_2O_3$ ($Co_2Y$) $BaO.6Fe_2O_3$ (BaM) powders were formulated utilizing chemical precipitation techniques. Materials were illustrated by manipulating X-ray diffraction (XRD), thermo-gravimetry (TG), differential thermal analysis (DTA) and Fourier transform infrared spectroscopy (FTIR). It was found that the BaM phase was formed directly

through the reaction of the preceding $Fe_2O_3$ and amorphous $BaCO_3$ for BaM precursor [102].

*P. Sharma et al.* in 2008 studied the Structural, Mossbauer and magnetic characteristics of Mn-substituted barium hexaferrites prepared by thermal annealing and high energy ball milling [33]. Due to the dilution of magnetic structure the magnetization decreases on increasing the substitution amount of dopant. The increase in coercivity is due to the decrease in lattice parameter 'c' which may increase the super exchange interaction between neighboring ions.

*P. Mohsen* in 2010 studied Barium hexaferrite synthesis by oxalate precursor route. The annealing temperature was kept at 800 to $1200^{O}C$ as the molar ratio of $Fe^{3+/}Ba^{2+}$ was controlled at 12. The resultant powders were investigated by X-ray diffractometer (XRD), differential thermal analyzer (DTA), vibrant sample magnetometer (VSM) and scanning electron microscopy (SEM). At annealing temperature of $1200^{o}C$, single well crystalline BaFeO phase was resulted. The SEM results showed that the grain particles were in regular hexagonal platelets shape. In addition, at $1100^{O}C$ annealing temperature; maximum saturation magnetization (66.36 emu/g) was also obtained.

*Yue Liu, Micheal G.B. Drew, and Ying Liu* in 2011 studied the " Preparation and magnetic properties of barium ferrites replaced with Nickel, cobalt and tin." Barium ferrites doped with Mn-Sn, Co-Sn, Mn-Co-Sn having general formulae $BaFe_{12}$-$2_xMn_xSn_xO_{19}$ formulated by an earlier stated co-precipitation technique. Low coercivity temperature coefficients, which can be modifiable by doping, were attained by Mn-Sn Mn-Co-Sn substitutions. By improving production method, relatively higher Ms values were also resulted [36].

*Yue Liu and Yang Li* in 2011 studied the arrangement data of barium hexaferrite and approaches for its synthesis. For highly effective synthetic designing along with tailoring the magnetic attributes of barium hexaferrite by doping, this arrangement knowledge is very crucial and in. M-type arrangement data has also assisted in finding the latest effective routes of hydrothermal and co-precipitation techniques for the formulation of barium hexaferrites along with the change in their magnetic properties by doping [37].

*Pratap Behera et al.* carried out a study in which nickel doped barium hexaferrite was synthesized by sol-gel method to form a single-phase polycrystalline sample. Dielectric properties were investigated using impedance spectroscopy at various frequencies to understand the relaxation mechanism of charge carriers. With increasing nickel concentration, dielectric constant seemed to increase while the tangent loss decreased. However, saturation magnetization decreased, and the transition temperature increased with increasing nickel concentration.

*Jun Young Kwak et al.* in 2012 studied the "characteristics of Barium Hexaferrite nanoparticles prepared by temperature-controlled chemical co-precipitation". By chemical coprecipitation, they prepared Ba-ferrite ($BaFe_{12}O_{19}$) nanoparticles in an aqueous solution. Synthetic condition of precipitation along with the calcination temperature are the factors that can control the Ba-ferrite nano-particles magnetic properties. Coercive force would be significantly reduced without a saturation magnetization loss when the Ba-ferrite nanoparticles were created by precipitation and calcination both at minimal. [39].

### 2.1.3 M Type Barium Hexaferrite:

M-type Barium Hexaferrite, a most commonly produced magnetic material globally, have a melting point of 1390$^{o}$C with magnetic coercivity of 160-255 kAm-1. Ferroxdure or BaM are the other names of M type barium hexaferrite. BaM found its applications in magnetic recording media, permanent magnets, and microwave devices [34].

### 2.1.4 Crystal Structure of M-type Barium Hexaferrite:

The composition of fundamental structural R and S blocks in BaM is $BaFe_6O_{11}$ and $Fe_6O_8$, respectively. R and S blocks are stacked in M type Barium hexaferrite to form a unit cell in sequence RSR*S* where the sign star denotes the 180$^{o}$ rotation about the c-axis of the hexagonal lattice. Therefore, two $BaFe_6O_{11}$ molecules are present in the unit cell of BaM. Four oxygen ions are present in each of the two hexagonal layers in S Block while R block constitutes three hexagonal layers of oxygen. One oxygen ion in the middle hexagonal layer in R block is replaced by a barium ion. Five interstitial sites are occupied by the metal

ions in the unit cell of BaM. The location of these sites, their sublattices, No. of ions and coordination's are mentioned in the table below [13]:

Table 2.1: Location, Sublattices and Coordination of Interstitial sites of BaM

| Block | Sublattice | Coordination | Ions per unit cell | Spin direction |
|---|---|---|---|---|
| | $4f_1$ | Tetrahedral | 4 | down |
| | $2a$ | Octahedral | 2 | Up |
| | $4f_2$ | Octahedral | 4 | Down |
| | $2b$ | Bi-pyramidal | 2 | Up |
| **S-R** | $12k$ | Octahedral | 12 | Up |

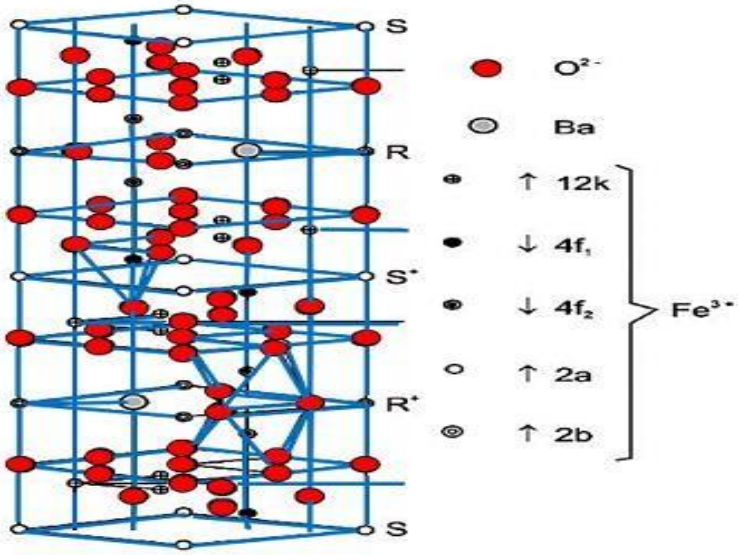


Figure 2.1: Unit cell of M type Barium Hexaferrite with the spin orientation of sublattices

# Chapter 3

# Materials and Methods:

# Synthesis Routes for Ferrites:

The two basic approaches used for the synthesis of nanoparticles include:

- Top-down approach.
- Bottom-up approach.

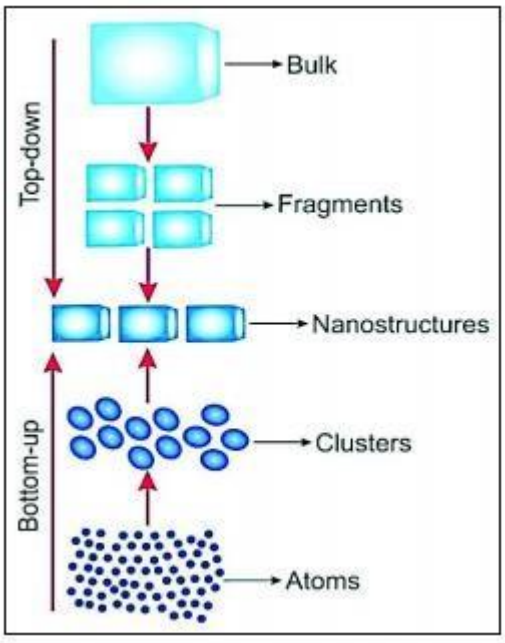


Figure 3.1: Schematic representation of fabrication of nano-structures using Top down and Bottom-Up approach

## 3.1 Top-Down Approach:

In this approach, Macroscopic initial structures are utilized and scaled down to fabricate many man-made materials including the semiconductor industry [36]. The typical example of this technique is lithography which is employed to print metal oxide field effect transistor onto silica wafer. Apart from advantages, the product obtains from topdown approach might contain significant amount of impurity.

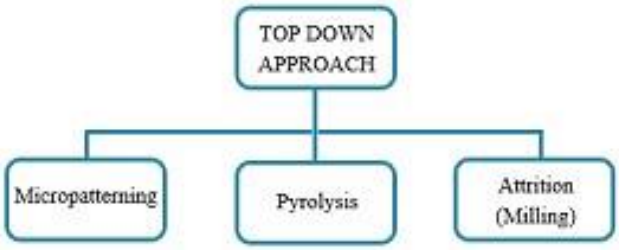


Figure 3.2: Examples of top-down approach

## 3.2 Bottom-Up Approach:

In contrast to top down, atoms and molecular are gathered to form nanoparticles which can be used to fabricate various intelligent nanodevices [36]. The drive behind the development of bottom-up approach is to mimic the self-assembled and self-organized preprogrammed biological structures and the supramolecular chemistry involved to combine those structures.

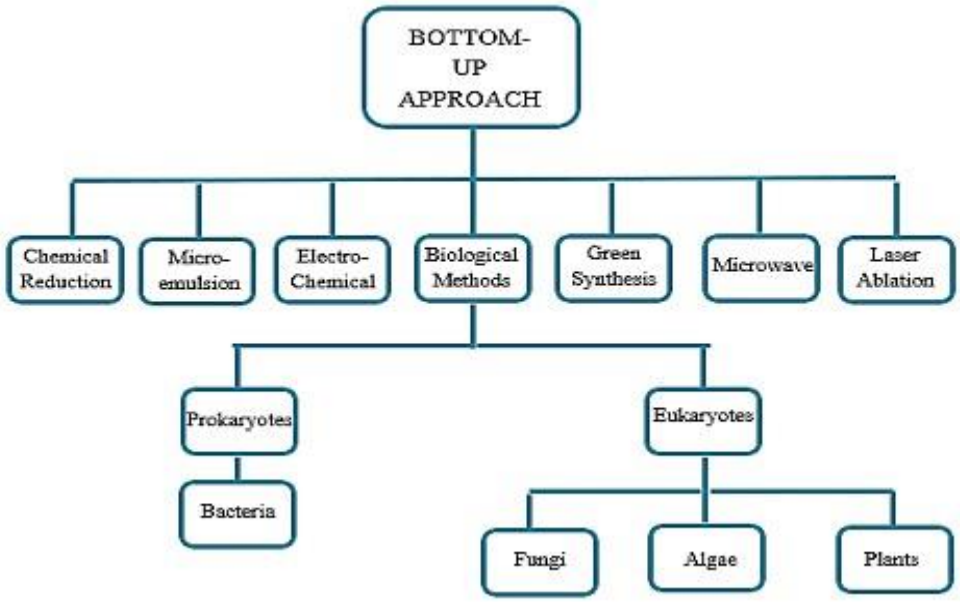


Figure 3.3: Examples of bottom-up approach

Synthesis of nanoparticles with nano dimensions have become very difficult task for many researchers. To obtain monodispersed nanoparticles, various methods have been adopted. These are listed as below.

### 3.2.1 Solid State Method:

In this method the constituent products are mixed collectively under elevated temperature. These methods are specifically employed for obtaining bulk material. Solid state reactions are often very slow, and their completion occurs at very elevated temperature [36]. The ferrites in bulk form are prepared through this method with size ranging in microns. Solid state approach also has some short comes such as chemical in-homogeneity, compositional control is poor, particle size is not fine and risk of impurities during grinding. To overcome these shortcomings chemical methods are implemented.

### 3.2.2 Chemical Method:

In this method the aqueous solution of the constituent's salt is used. The obtain solutions of these materials are then dried and fine powder is achieved. This method is also termed as wet method. The wet method or chemical methods have their advantages to design and manufacture new materials for refinement into final products. The main advantage of chemical method is its chemical homogeneity [36]. This method is based upon mixing of constituent at molecular level. Besides these advantages some hurdles also arise in chemical processing due to complex chemistry and hazardous nature. In some cases, contamination may result from by product being produced or some side reactions may take place. Agglomeration can cause severe problems in any step of synthesis & development and significantly changes properties of material. Fine nanoparticles can be synthesized by precipitation from precursor solutions which is common technique for the synthesis. When the supersaturated solution is formed, precipitates are formed either by homogenous or heterogeneous nucleation. By the process of diffusion, nucleation takes place. The concentration slope and the temperature of reaction are key factor to determine the growth rate of mono dispersed nanoparticles. Narrow size distribution is needed for un-agglomerated preparation of particles such that all the simultaneous formation of nuclei and their growth must occur subsequently [37]. Kinetics of reaction is influenced by preventing nucleation or agglomeration of the particle, distribution of the particle size, crystallinity, crystal structure and degree of dispersion. Also, the concentration of constituents, temperature of reaction, sequence of mixing of the reactant and the pH are also

essentials. To obtain chemical homogeneity and stoichiometry it is required to have careful controls on reaction conditions. Particle size of the ferrite nanoparticles is key parameter, playing key role to determine the magnetic and electrical properties.

Different methods in preparing ferrite nano particle are listed below:

1. Sol-Gel Method
2. Combustion Flame Synthesis
3. Co-precipitation
4. Mechanical alloying Technique
5. Micro emulsion Method
6. Sono-chemical Method
7. Hydrothermal method

In our research work Sol-gel method was employed successfully for preparation of $Ba_{12-x}Ni_xCo_xFe_{12}O_{19}$ ferrite nano particles.

## 3.3 Sol-Gel Method:

Sol-gel method is utilized in this study to synthesize M-type Barium Hexaferrite doped with cobalt and nickel at x = 0, 0.1, 0.175, 0.25. During the process, a gel is formed which provided high degree of homogeneity and the diffusion of atom is reduced in the solidstate calcination. This technique provided better control on products and cost effective. The materials which are made through this technique have wide applications in optics, electronics, and energy etc.


Figure 3.4 Sol-gel method to synthesize various forms of materials.

## 3.4 Materials:

Below are the details of the experiment carried out to prepare the desired sample.

Table 3.1 Chemicals and their Formulas

| | **Name of Chemical** | **Formula** |
|---|---|---|
| 1 | Barium Nitrate | $Ba\ (NO_3)_2$ |
| 2 | Iron Nitrate Nonahydrate | $Fe\ (NO_3)_3.9H_2O.$ |
| 3 | Cobalt Nitrate Hexahydrate | $Co\ (NO_3)_2.6H_2O.$ |
| 4 | Nickel Nitrate Hexahydrate | $Ni\ (NO_3)_2.6H_2O$ |
| 5 | Citric Acid | $C_6H_8O_7$ |
| 6 | Ammonia Solution | $NH_4OH$ |

Initial reagent to synthesize all the salts is deionized water. All the chemicals used for samples preparations in this study were of purity ≥ 99% and were used without any further purification.

### 3.4.1 Synthesis of Barium hexaferrite ($BaFe_{12}O_{19}$):

Sol-gel method was used to synthesize $BaFe_{12}O_{19}$ and the stoichiometric formula that was used to calculate mass for three different compositions of different chemicals utilized in the process is as follows:

$$\frac{Molarity \times Molecular\ mass \times 100}{1000} \quad \text{.....(3.1)}$$

Solution of Barium nitrates Ba $(NO_3)_2$ and iron nitrate (III) nonahydrate Fe $(NO_3)_3.9H_2O$ were prepared according to their stoichiometric ratios. Ba $(NO_3)^2$, Fe $(NO_3)^3.9H_2O$ were dissolved in 200 ml of deionized water by constantly stirring using a magnetic stirrer for 15 minutes for their complete dissolution and to get clear solution in water. 200ml of deionized water was taken to dissolve citric acid and was stirred until solution get clear and complete dissolution took place [38]. In a large beaker both solutions were added with continuous stirring using magnetic stirrer and after 15 minutes of stirring pH was neutralize by adding ammonia solution. Continuous stirring of solution was done and then the solution was heated at 90°C is powered ON, with the same condition of stirring. After some time, the solution started to change in to gel form. Finally, the thickened gel catches fire in beaker and once the combustion was completed, heating and stirring was turned off. Dark brown colored powder was obtained after combustion [37]. The powder was grinded in mortar and pestle and then calcination of the collected powder was done at 950$^o$C for 5 hours.

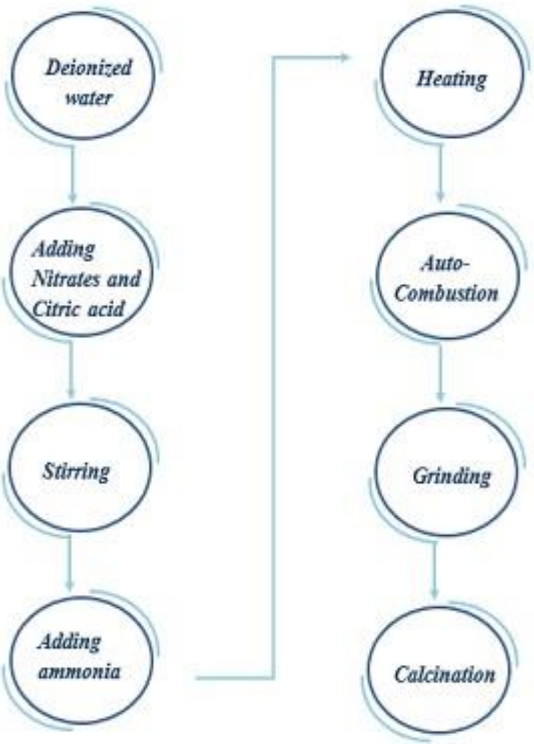


Figure 3.5 Flow chart of the Synthesis of Pure Barium Hexaferrite

## 3.5 Synthesis of $BaFe_{12}O_{19}$ doped with Nickel and Cobalt dopant: $Ba_{1-2x}(Ni_x, Co_x)Fe_{12}O_{19}$:

Series of sample preparation with cobalt & nickel as a dopant was prepared. The sample series [$Ba_{1-2x}$ $Ni_x$ $Co_x$ $Fe_{12}O_{19}$] for x=0, 0.1, 0.175, 0.25, were prepared. Samples were prepared in 600 ml of deionized water by adding Ba $(NO_3)_2$, Fe $(NO_3)_3.9H_2O$, Co $(NO_3)_2.6H_2O$, Ni $(NO_3)_2.6H_2O$ and citric acid according to their stochiometric ratios by sol-gel technique. The solution was continuously stirred for 15 minutes with magnetic stirrer until the complete dissolution took place solution became clear. Dropwise solution of ammonia was added until the pH reaches 7 with continuous stirring. Solution was stirred continuously with magnetic stirrer and then heating at 90°C temperature is powered ON, with the same condition of stirring [38]. After some time, the solution started to change in gel form and after thickened gel catches fire in beaker and after complete combustion the heating and stirring is stopped. After combustion, dark brows colored powder was obtained. Grinding was done and then placed in muffle furnace at 950 °C for 5 hours for calcinations purpose.

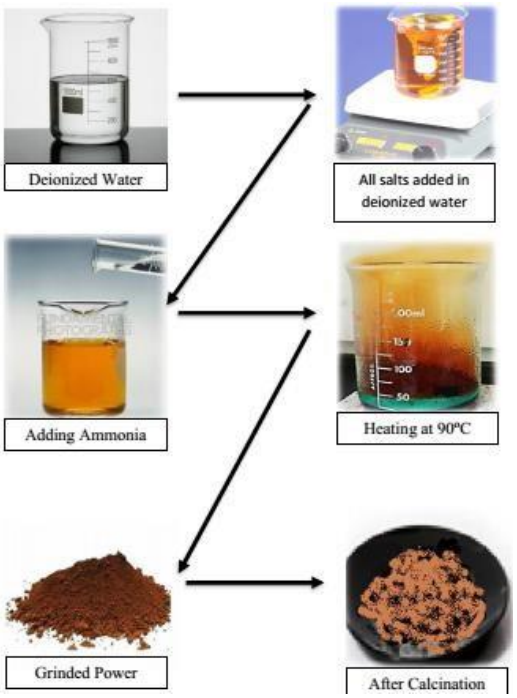


Figure 3.6: Flowchart of Synthesis of BaM doped with Ni, Co.

# Chapter 4

# Characterization Techniques:

The properties of synthesized nickel ferrite nanoparticles with graphene loadings are analyzed by performing some specific analysis techniques [39]. Properties like physical and chemical properties and other information about material such as morphology, lattice parameter, structure etc. can be obtained using one of the analysis techniques. This chapter will cover a short introduction of the characterization techniques. Following characterization techniques can be used for the analysis of synthesized composite.

## 4.1 X-Ray Diffraction Technique:

It is a useful tool for the identification of degree of crystallinity and structure of a material. Clear information about structural strain, crystal defects, average crystallite size, crystallographic orientation and degree of crystallinity can be obtained using XRD [32]. Three different methods can be used for finding out crystal structure i.e., Powder diffraction method, Laue method and Rotating crystal method. Two techniques can be used to determine crystal size if powder diffraction method is used. Those techniques are as follows.

- Debye Scherrer Method.
- Diffractometer method the sample was in the form of fine grinded powder. Copper, Molybdenum etc. can be used as a target material. Cu kalpha=1.54 Å source was the XRD source used for analysis in this case.

### 4.1.1 Basic Principle of XRD:

The powdered sample is placed for analysis. X-ray beam is made to fall on the sample and reflected from plane of crystal [40]. The crystal plane reflects the X-rays that are incident on material. The interference only takes place when incidence angle is exactly same as reflection angle. The Bragg's Law is given by.

$$n\lambda = 2d\sin\theta \quad \text{.....(4.1)}$$

n is order of interference, θ is incidence angle, d is Interlayer distance and λ is incident X-ray wavelength. The Bragg's law states that the incident ray is reflected only when the path difference between set of planes is 2dsinθ [33]. The set of planes are at an equal distance of d. Following is the condition required for constructive interference:

$2d\sin\theta = n\lambda$, where n=1,2,3….

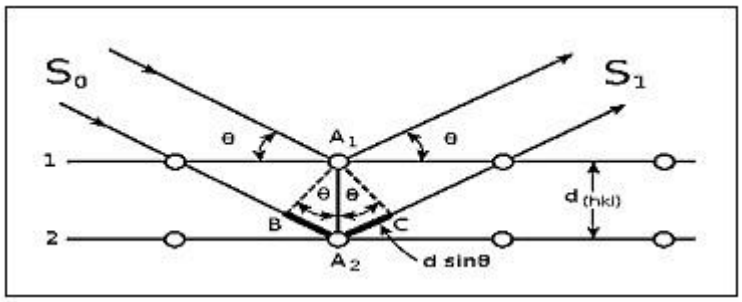


Figure 4. 1: Incident x-ray beam scattered by atomic plane in a crystal.

The equation is known as Bragg's equation. The condition for reflection in above mentioned equation is that it only occurs when θ<2d. For this reason, visible light cannot be used. For the characterization of a three-dimensional structure three techniques are usually used which are as follows:

- Laue Method
- Powder method
- Rotating Crystal Method

The sample which is to be characterized using XRD is in the form of Nano powder. So, the powder method will be the one useful for the desired sample [41]. For the evaluation of powdered sample and in the case of in availability of single crystal of acceptable size, powder diffraction is the best method to be employed. The procedure of this experiment includes the crushing of sample into fine powder. Afterwards the sample will be placed in aluminum or glass rectangular shaped plate. A monochromatic X-ray beam is then directed towards the powdered sample [41].

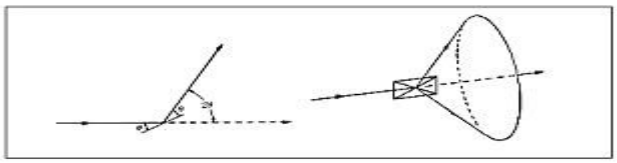

Figure 4. 2: Image showing monochromatic X-ray beam

### 4.1.2 X-Ray Diffraction:

Consider the reflection as shown in figure. The fraction of sample, which is in powder form, is at such an orientation which will enable reflection by being present at correct Bragg angles [42]. When the plane is rotated about the beam which is made incident, the path of motion of reflected beam will be across the surface of cone. In the case of our particles the reflection does not occur across the surface, many crystal particles will have same reflections and some of those reflections will be able to satisfy brags law [42]. The inter planner spacing, d, can be calculated by knowing values of λ and θ.

### 4.1.3 Lattice Constant:

Lattice constant defines the unit cell of a crystal. The distance, which is constant, between the lattice points is known as lattice constant. Following equation is used to calculate lattice constant.

$$\frac{1}{d^2} = \frac{4}{3}\left(\frac{h^2+hk+k^2}{a^2}\right) + \frac{l^2}{c^2} \quad \text{……..(4.2)}$$

In the above equation, lattice constant is “a”, the wavelength of X-ray radiation is 1.54 for Cu-kα, miller indices are “h, k, l” and diffraction angle is θ.

### 4.1.3 Crystallite Size:

For the identification and confirmation of the experimentally obtained diffraction pattern it is compared to JCPDS cards [43]. The structural properties are greatly influenced by particle size. According to Debye Scherrer equation, which is used to calculate 41 particle size, crystal size is inversely proportional to peak width. So, the small crystallite size is related to peak broadening in XRD analysis. The Debye Scherrer equation is used to calculate particle size.

$$t = 0.9\,\lambda\,\beta\,\cos\theta \quad \text{…….. (4.3)}$$

### 4.1.4 X-Ray Density:

The X-ray diffraction data can be used for the calculation of sample material's density. If the lattice constant is known for each sample following formula will be used [43].

$$\rho_x = n.M_w / (N_A.V) \quad \text{……..(4.4)}$$

### 4.1.5 Porosity Fraction:

Along with the alternation in compositions, the increase in the porosity fraction is observed. Following formula is used for calculation of porosity fraction.

$$\text{Porosity Fraction} = 1 - \rho m\ \rho x \quad \text{…….. (4.5)}$$

## 4.2 Fourier Transform Infrared Spectroscopy:

The absorption, emission spectra's, Raman scattering, and photoconductivity of the material can be obtained by using this analytical technique [45].It collects the data from spectrum of matter. FTIR is used to determine the amount of light that a sample absorbs at a specific wavelength [44].

### 4.2.1 Working of FTIR:

In Fourier transform infrared spectroscopy, a source of infrared light which is polychromatic is made to fall on splitters [45].The information about molecular component and structure of the sample can be obtained by interaction of light with sample.

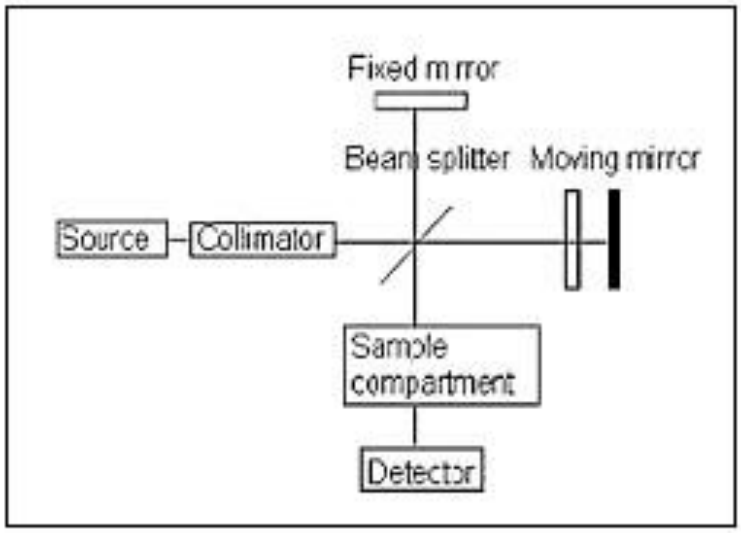


Figure 4. 3: Schematic figure of Fourier transforms spectroscopy.

It is a sensitive technique and can also be used for identification of many organic compounds for example, paints, polymers, resins, coatings, and drugs etc. it is the only analytical technique which provides ambient temperature operation and capability of monitoring the vibrations of functional groups directly, which are used for characterizing molecular structure and governing the course of chemical reactions [46].The higher the temperature, more the atoms move producing more IR radiations. According to the principle of FTIR, molecular vibrations are produced because of absorption of IR radiation when the applied IR frequency is equal to the natural frequency of vibration. Different frequencies are required by every different bond or functional groups for absorption. Therefore, the characteristics peak is observed for every functional group or part of the molecule.

### 4.2.2 Applications of FTIR:

- The analysis of liquid chromatography fraction can be done using FTIR.
- Tiny samples can be checked with the help of infrared microscope in sample chamber.

## 4.3 Scanning Electron Microscopy:

SEM is an important instrument that nanoscience researchers use in their daily routine for the characterization of nanomaterials. When we are talking about organic and inorganic materials in nanoscale then with the help of SEM [47]. SEM

is possible to attain images of any materials. In SEM we study topographical and morphological by sending an electron on surface then we will study that emitted electron from surface. We can also analysis the composition of any material by observing that will be produced by electron specimen interaction. In sensors technology, SEM is predominantly used to observe sensing layers and surface and thin films [49].

Schematic diagram of SEM is shown. Basic principle is that an electron will emit from heated filament and that filament is made of lanthanum hexaboride or it will be tungsten. We can heat this filament by applying voltage and then electrons will be emitted. We can also emit these electrons by field emissions. Now by applying voltage we can accelerate electrons towards sample [48]. The electron beam focused by condenser lens that will project image of source onto condenser aperture.

### 4.3.1 Working Principle:

In the result there will be emission of secondary electron. Energies of these secondary electrons will be very low. Secondary electrons will be collected by a detector named Everhart Thomley [50].At very low-pressure scanning takes place then electrons will not scatter by molecules of gas inside chamber. By using SEM, it is also possible to get image from large of sample. SEM can also monitor formation and growth of the thin films. In research SEM takes place an important role because its help scientists to understand interaction between sensing layer and analytic, because sensitivity strongly depends on topography and surface morphology. SEM is designed for special purpose which ranges from cryogenic studies, morphological studies, and high-speed compositional analysis and for study of environment sensitive materials [49].

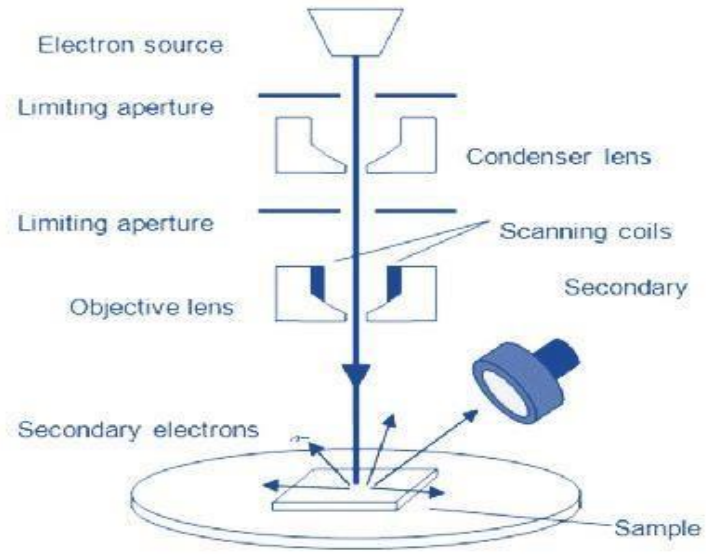


Figure 4.4: Schematic diagram of SEM

## 4.4 Electrical Properties:

Dielectric properties are measured using impedance analyzer pellet is placed in pellet holder and connected to device [53].

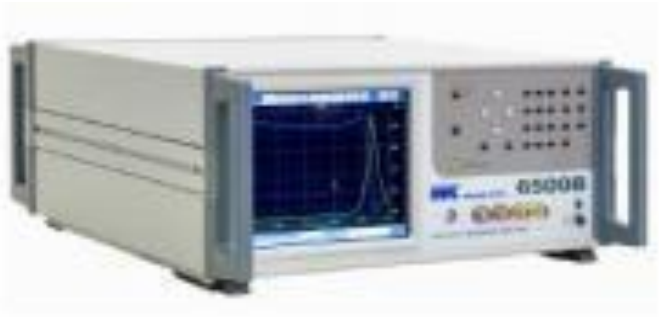

Figure 4.5: Impedance analyzer

### 4.4.1 Dielectric Properties:

The LCR meter bridge is used for determination of dielectric properties such as dielectric loss, dielectric constant etc [52]. Firstly, the capacitance of pallets was found out using LCR meter then following formula is used for the calculations of dielectric constant [51].

$$\varepsilon' = Cd/A\varepsilon_{\circ} \quad \ldots\ldots\ldots \quad (4.6)$$

There are different types of polarization which take place in dielectric materials when the Interact with the applied field [52].

### 4.4.2 Electronic and Atomic polarization:

When the dielectric material is placed within the electric field the electron cloud of atoms is displaced relative to nuclei in atom, which produce an induced dipole moment in the molecule.

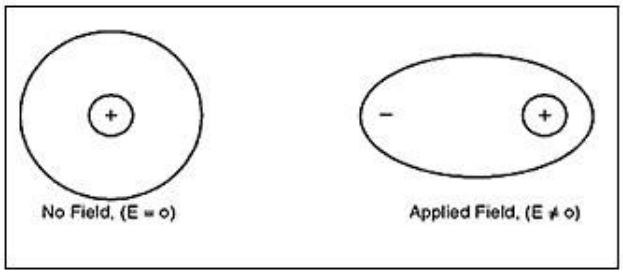


Figure 4. 6: Electronic polarization

### 4.4.3 Ionic Polarization:

Ionic polarization take place in solids with ionic bonding having dipoles, but these dipoles get cancel due to the symmetry of the crystals structure [53]..

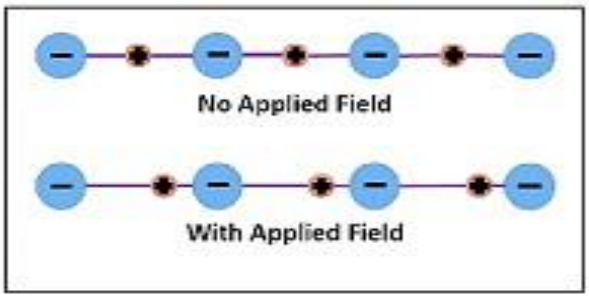


Figure 4. 7: Ionic polarization

### 4.4.4 Dipolar and Orientation Polarization:

It is only applicable to the polar dielectric materials. In the absence of electric field dipoles are randomly oriented so the sum of their dipole moment is zero [54]. When these polar dielectric materials are placed within the electric field these dipoles rotate and align themselves in the direction of electric field.

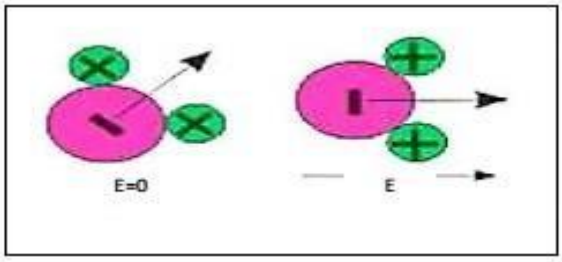


Figure 4. 8: Dipolar Polarization

### 4.4.5 Interface and space charge Polarization:

Space charge polarization take place due to the diffusion of ions along with applied electric filed [54].

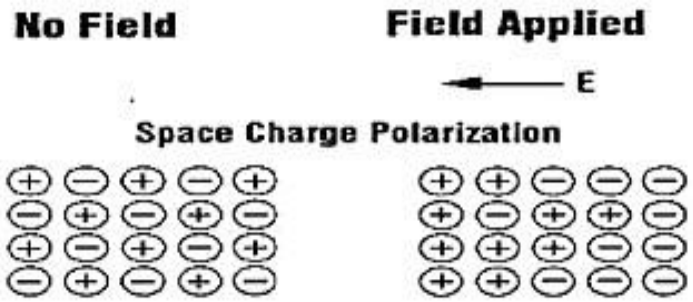


Figure 4. 9: Space Charge polarization

### 4.4.6 Dielectric Constant:

It is an ability of the material that expresses the force between two-point charges. It is the factor by which the electric field is decreased between the charges relative to vacuum. The dielectric parameters can be explained according to Maxwell-Wagner model and Koop's theory

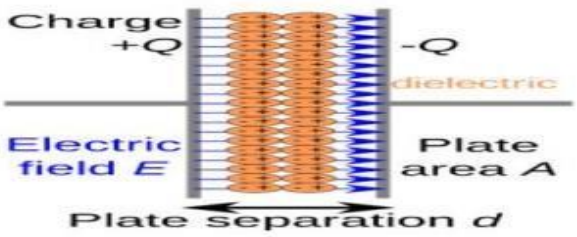


Figure 4.10: Dielectric Dipole [46]

### 4.4.7 Dielectric Loss:

It is also known as the imaginary part of dielectric that corresponds to energy dissipation and calculated by the equation.

**Dielectric Loss Tangent:** This shows energy dissipation . It is the ratio of dielectric constant and dielectric loss as shown by the equation.

**AC Conductivity:** Happens because of the mechanism of hopping. It is calculated using the equation.

**AC Impedance:** Parameters of the samples were measured at room temperature. Resistance (R) and reactance (X) were measured over a range of 100 Hz to 5 MHz frequency. The impedance is a complex quantity where resistance (R) and reactance (X) shows the real and imaginary parts of impedance in the circuit by the relation: The impedance shows the resistive behavior of the material. The SI unit of impedance is 'Ω'.

Figure 4.11: LCR Meter

## 4.5 Ultraviolet/visible spectroscopy:

UV visible spectrometer is a device through which absorbance of visible or ultraviolet light by a specimen can be studied. As it is known that visible light contains a spectrum of electromagnetic radiation having both electric and magnetic portions. However, UV visible spectroscopy only deals with electric portion that is why also known as electronic spectroscopy. The basic principle of this technique is absorption of certain amount of energy which results in the transitions from lower energy to higher energy levels. UV region lies in the range of 190 nm to 400 nm while visible lies in the range of 400nm to 800 nm. The short UV spectroscopy works in the range of 200 nm-800 nm and transition in energy level occurs when absorption of light occurs in this range.

There are various transitions due to absorption of light occurs from highest occupied molecular orbital (HOMO) to lowest unoccupied molecular orbital (LOMO). Lowest energy orbitals correspond to s-orbital denoted by sigma (σ) bonds while higher energy orbitals relate to p-orbital denoted by pie (π) bonds. Non-bonding orbitals are higher energy levels as compared to p-orbital while antibonding pie ($\pi^*$) and sigma ($\sigma^*$) are the highest. Transitions due to light absorbance are shown in fig 3.7.

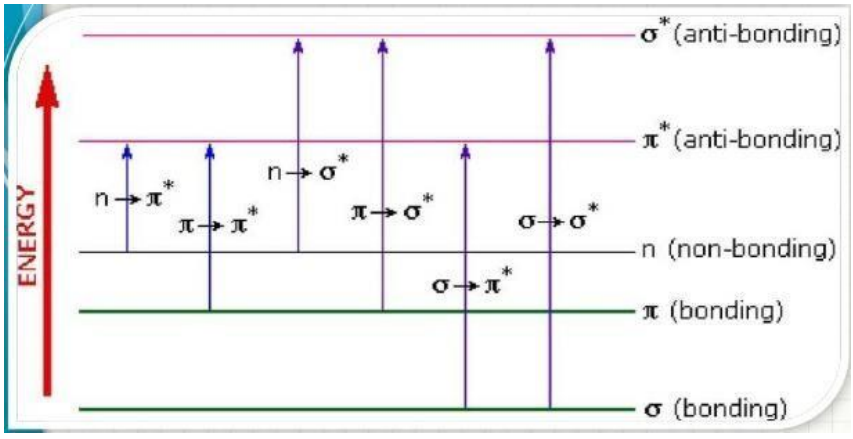


Figure 4.12: Electronic transition spectrum

### 4.5.1 Construction and Working Principle:

To cover the whole UV and visible range the source is made up of tungsten, halogen and deuterium lamps. Tungsten generates the rays having wavelength >375 nm while halogen and deuterium covers the range <375 nm. It contains a monochromator having slits and prism. These rotating Prism are used to scatter radiations while slits separates single beams which are monochromatic and with the help of another prism these beams are further divided into two more beams. One of these two beams is passed from refrence solution while the other beam through sample solution. A cell contains both the solutions made up of quartz and silica. While two detectors are used having photocells. Beams from sample cell and reference cell are received by these two detectors. The beam generated by sample cell is stronger and alternating current in photocell is produced. While amplifier next to detector is used to enhance the signals received. While in the end a pen recorder is installed parallel to amplifier directly connected to computer that is used to store data and spectrum depiction. [60from thesis]

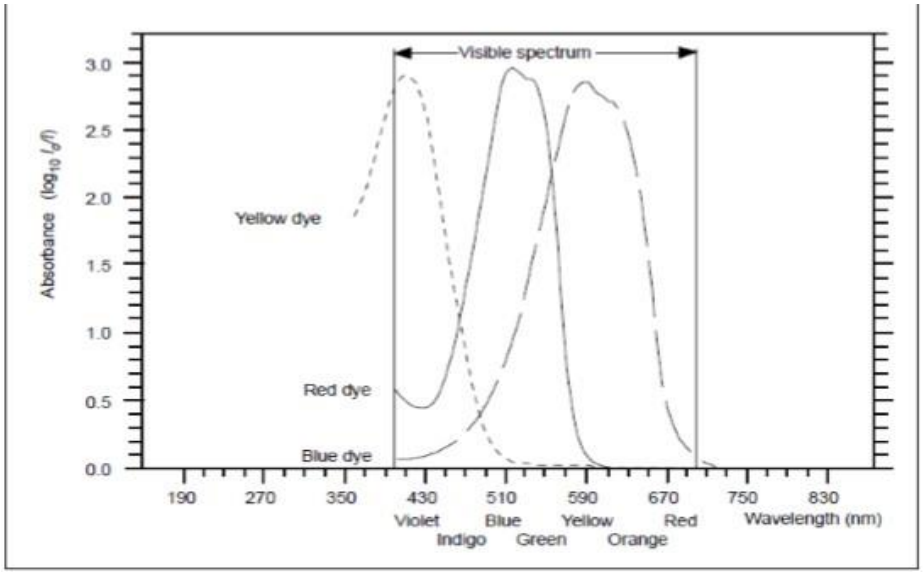


Figure 4.13: Absorption of light by dyes

From Beer's law, the absorption depends upon the absorbing molecules (for dilute solutions only) i.e the absorption is directly proportional to the concentration of

absorbing molecules. While from lambert's law, radiations which are absorbed are independent of their intensity. From these two laws beer-lambert law is introduced

$$Log_{10} I_o / I = \varepsilon lc \ldots\ldots\ldots\ldots\ldots\ldots (4.7)$$

Where $I_o$, I, ε, l and c represents the radiation intensity, transmitted radiation intensity, molar absorption coefficient, absorbing solution path length and absorbing molecules concentration.

The value for $\log_{10} (I_o/I)$ represents the solution absorbance which can be directly studied from the spectrum. Absorption constant called as molar absorption coefficient does not depend upon concentration and path length while absorption is dependent of both the concentration and path length.

While another important information can be calculated from $\lambda_{max}$, which is the maximum absorption at certain wavelength. If ε and $\lambda_{max}$ are known Solution concentration can be calculated, while both the terms depend on solution nature.

### 4.5.2 Applications for UV spectroscopy:

- UV spectroscopy used to find out impurities in samples.
- It can also use to find out the functional group present in compound, absence of wavelength shows absence of specific functional group.

## 4.6 Vibrating Sample Magnetometer (VSM):

Simon Foner, in 1959 designed the first Vibrating sample Magnetometer at Lincoln Laboratories. Its main purpose is to measure the routine magnetic properties at varying temperatures for all type of magnetic materials like Ferrimagnetic, Ferromagnetic, antiferromagnetic, diamagnetic, and paramagnetic.

### 4.6.1 Principle:

Vibrating sample magnetometer work on the principle of Faraday's law of Induction according to which a homogeneous magnetic field is applied on the sample and is vibrated at a small, fixed amplitude. The pick-up coils are stationary

with respect to vibrating sample. The change in applied magnetic field generates voltage in stationary pick-up coils.

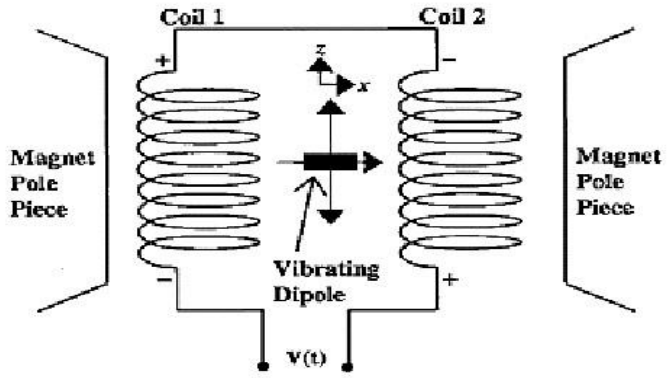


Figure 4.14: Principle of Vibrating Sample Magnetometer

### 4.6.2 Parts of VSM:

- **Water cooled electromagnet:** The constant magnetic field used to magnetize a sample is provided by water cooled electromagnet along with power supply.

- **Sample holder and Vibration exciter:** A sample rod is used to hold the sample between pick-up coil pole pieces. Sample rod is attached to a vibration exciter which vibrate the sample with a fixed frequency. Different orientation of the sample can be exposed to constant magnetic field by rotating the sample rod. Oscillation of the vibration exciter is controlled by a chassis.

- **Sensor Coils and Amplifier**: As the sample is vibrated at a fixed frequency, alternating current is generated in these sensor coils. Signals generated through sensory coils are amplified by the attached amplifier to confirm the magnetization of the sample.

- **Lock-in Amplifier**: This amplifies the signals by removing the noise coming from environment and only catches the signals only vibrating sample.

- **Computer interface**: Data collection is made easier by the use of the software as it controls various components during the process.

# Chapter 5

# Results and Discussion:

## 5.1 XRD Analysis:

XRD analysis was performed for phase testing and structural information. The sample was finely grounded and annealed at 950oC before subjecting to XRD analysis.

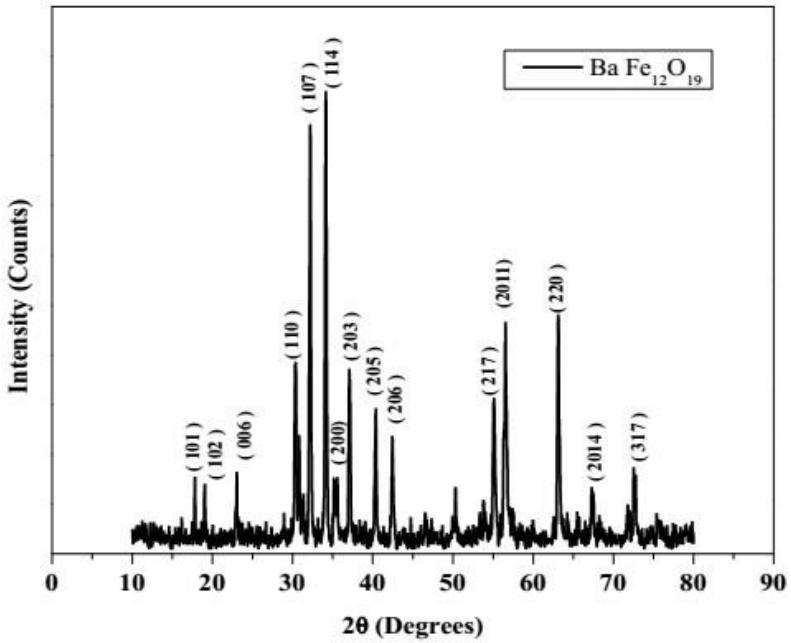


Figure 5.1: XRD Pattern of pure Barium hexaferrite

Fig 5.1 represents the XRD peaks of pure barium hexaferrite. The well-separated diffraction peaks for all the samples appear at planes (101), (102), (110), (008), (107), (114), (200), (203), (205), (206), (209), (217), (303), (304), (20 11), (220), (20 14), and (317) present at angles of 2θ = 17.784, 18.988, 30.315, 30.831, 32.196, 34.113, 35.146, 37.078,40.316, 42.422, 50.295, 55.057, 55.256, 56.326, 56.598, 63.06, 67.362 and 72.585 respectively [56]. The pattern of peaks at specific angle matches with JCPDS 50 data card No. 84-0757. The absence of any secondary peak confirms that there is no extra hematite phase. Hence shows the completion of the reaction. XRD analysis shows the barium hexaferrite nanoparticles exhibit a single-phase hexagonal structure [55].

### 5.1.1 Barium Hexaferrite doped with Co, Ni [$BaFe_{1-2x}O_{19}$]:

The Barium hexaferrite was doped with Nickel, Cobalt, and nickel with various concentrations where x = 0, 0.1 0.175, 0.25 using the sol-gel method for synthesis. XRD analysis was performed for the prepared doped samples after annealing at 950$^{o}$C. The miller indices h, k, and l of the XRD peaks for the synthesized compound matches with the barium hexaferrite JCPDS data card No. 84-0757.

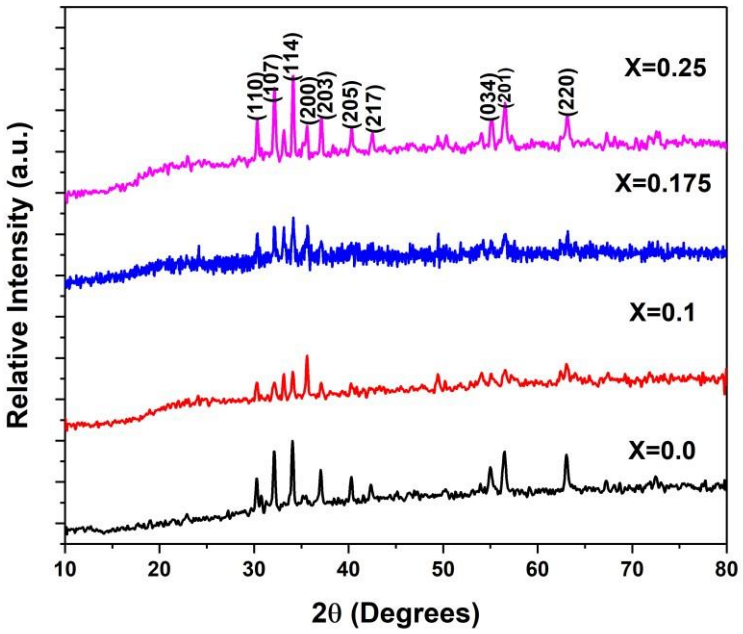


Figure 5.2: XRD Pattern of Ni, Co doped Barium hexaferrite $BaFe_{1-2x}O_{19}$

There is no separate peak found after the doping of metallic cations Ni and Co because of minimalistic difference in ionic radii of $Fe^{+3}$ and $Ni^{+2}$, and $Co^{+2}$. The ionic radii of $Fe^{+3}$ is 0.60 $A_o$ while the ionic radii of $Ni^{+2}$ and $Co^{+2}$ is 0.69$A_o$ & 0.70 $A_o$ respectively. so, as the ionic radii of three metallic cations and iron were comparable suggesting that the cations replaced iron-on tetrahedral sites. The following relation was used to calculate the lattice parameters of pure and doped samples [56].

$$\frac{1}{d^2} = \frac{4}{3}\left(\frac{h^2+hk+k^2}{a^2}\right) + \frac{l^2}{c^2} \quad \text{..... (5.1)}$$

Where a and c represent the lattice parameters. h, k, and l are the miller indices of identified peaks while the d represents the d-spacing between two lattice planes. With the addition of metallic cations as the dopant in barium hexaferrite, a slight change in lattice parameters was observed, probably because of minute change in ionic radii of iron and metallic cations [57].

Table 5.1: Lattice parameters of Pure and Doped BaM

| **Sr. No.** | **Prepared Sample** | **Lattice parameters** | | **Crystallite Size** |
|---|---|---|---|---|
| | | **a=b** | **c** | |
| **1** | $Ba_{1-2x}Ni_xCo_xFe_{12}O_{19}$ where x=0.0 | 5.58 | 24.03 | 37 nm |
| **2** | $Ba_{1-2x}Ni_xCo_xFe_{12}O_{19}$ where x=0.1 | 5.51 | 21.03 | 40 nm |
| **3** | $Ba_{1-2x}Ni_xCo_xFe_{12}O_{19}$ where x=0.175 | 5.46 | 20.03 | 44 nm |
| **4** | $Ba_{1-2x}Ni_xCo_xFe_{12}O_{19}$ where x=0.25 | 5.79 | 23.03 | 55 nm |

## 5.2 Fourier Transform Infrared Spectroscopy:

FTIR analysis was performed in the range of 4000 $cm^{-1}$ to 350 $cm^{-1}$ to understand the nature of chemical bonds present in the prepared sample. The figure shows the FTIR peaks of pure and doped barium hexaferrite [58]. Sample for FTIR analysis was prepared by homogenous mixing of sample and potassium bromide and then the powder is converted into pellets. It can be inferred from analyzing the peaks that the nature of chemical bonds in all the samples is the same as the peaks are almost undifferentiable. These absorption bands are attributed to the vibrations of sub-lattices present in the hexagonal structure of barium hexaferrite

i.e. tetrahedral and octahedral sub-lattices [58]. Metal and oxygen bonds, present in the tetrahedral and octahedral sub-lattices, cause the stretching and bending vibrations resulting in the absorption bands. The position of the band for the octahedral and tetrahedral site differs slightly because of the difference in bond length of Fe-O. Tetrahedral ($v_1$) and Octahedral ($v_2$) frequency bands correspond to the tetrahedral and octahedral sites in barium hexaferrite, respectively [58]. The vibrational frequency of the tetrahedral site is higher than the octahedral site because the bond lengths in the tetrahedral site are shorter. As the dopant concentration is increased from x= 0.0 – 0.25, the tetrahedral vibration frequency-shifted toward a lower frequency range. This behavior can be attributed to the replacement of $Fe^{+3}$ ions by the dopant metallic cations. As the bond length increases at the tetrahedral sites, the vibrational frequency is shifted toward the lower range [59].

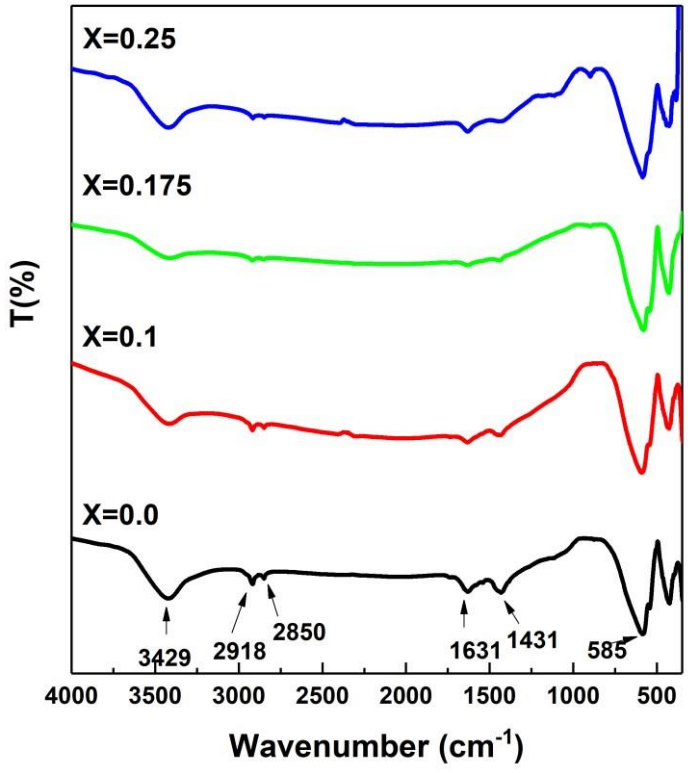


Figure 5.3: FTIR of Pure and Doped BaM ($BaNiCoFe_{12}O_{19}$)

## 5.3 Scanning Electron Microscopy:

SEM technique is used for microstructure analysis. It provides useful information about phase formation, grain/crystalline size & composition of sample. It is also useful to interpret about porosity of the sample materials. Suspension of the samples for analysis was prepared using deionized water and sonicate for 3 hours. Fig 5.4 shows the SEM images. The images shows that the sample prepared have spherical uniform distribution while some agglomeration can be seen in some samples due to deprived sonication. Concentration of samples was x=0.0, 0.1 ,0.175, 0.25. Particle size found to be in the range of 80nm to 44nm.

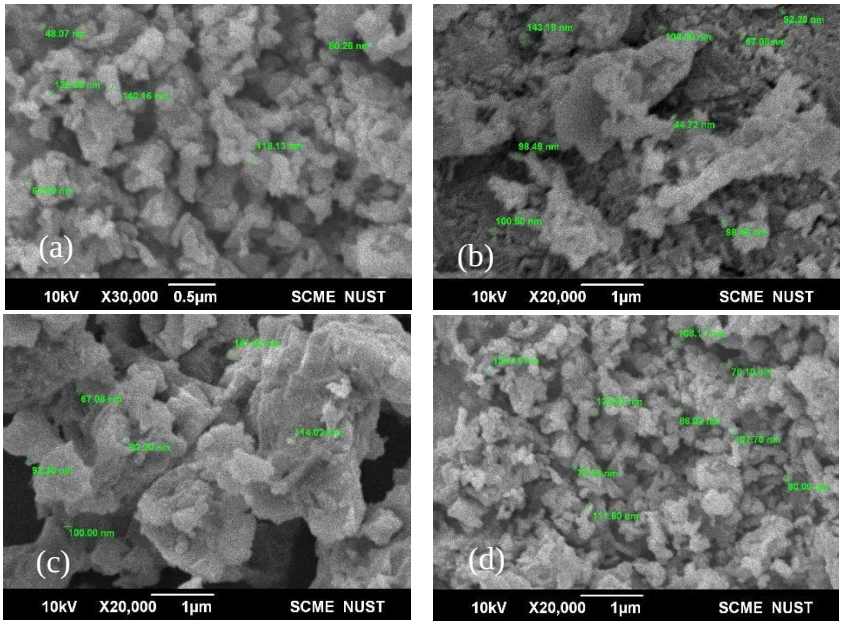


Figure 5.4: SEM of Pure and Doped BaM ($Ba_{1-2x}Ni_xCo_xFe_{12}O_{19}$)((a) 0.0, (b) 0.1. (c) 0.175, (d) 0.25)

## 5.4 Magnetic Measurement:

Vibrating Sample Magnetometer (VSM) is a technique used to measure magnetic properties of a material. This is used to measure M-H loop for pure Barium ferrite and Barium doped Cobalt & Nickel ferrite up to the magnetic field of 10kOe as shown in

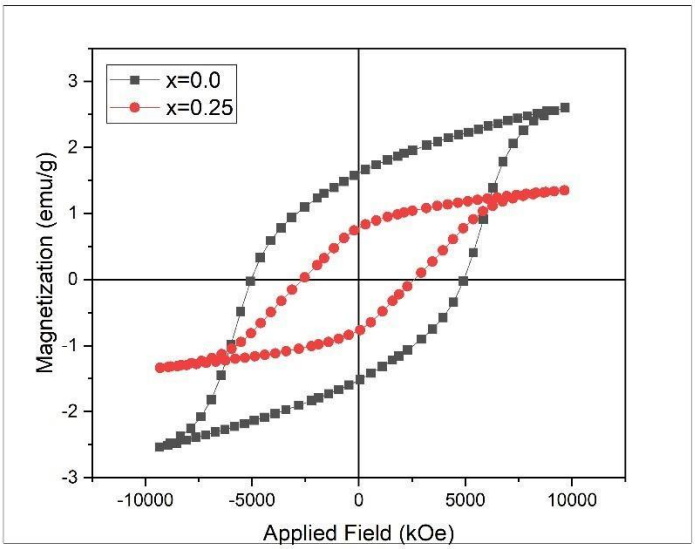


Figure 5.5: VSM of Pure and Doped BaM ($BaNiCoFe_{12}O_{19}$)

Table 5.2: Mr, Ms & Hc Pure and Doped BaM

| **Sample** | **$M_s$ (emu/g)** | **$M_r$ (emu/g)** | **$H_c$ ($kAm^{-1}$)** |
|---|---|---|---|
| $BaFe_{12}O_{19}$ | 2.569 | 1.569 | 4988.414 |
| $BaFe_{1-2x}(Ni, Co)_{0.25}O_{19}$ | 1.343 | 0.777 | 2617.815 |

## 5.5 Dielectric Studies:

The prepared sample powder was pressed into pallets using hydraulic press and then sintered at high temperature to analyze the Dielectric constant, dielectric loss, tangent loss, AC conductivity and AC impedance [60].

### 5.5.1 Dielectric Constant:

Dielectric constant is a result of polarization which can be either interfacial, dipolar electronic or ionic polarization. Dielectric constant has:

- Real Part.
- Imaginary Part.

The calculated value of dielectric constant for pure barium hexaferrite at 500hz is $2.29x10^{+2}$. Dielectric constant increased with increasing concentration of metallic cation dopants $BaNi_xCo_xFe_{12}O_{19}$. The highest value of dielectric constant 1.45 x $10^3$at 500hz came for x=0.25. The increasing trend of dielectric constant with increasing concentration of dopant at 500Hz is shown in figure below:

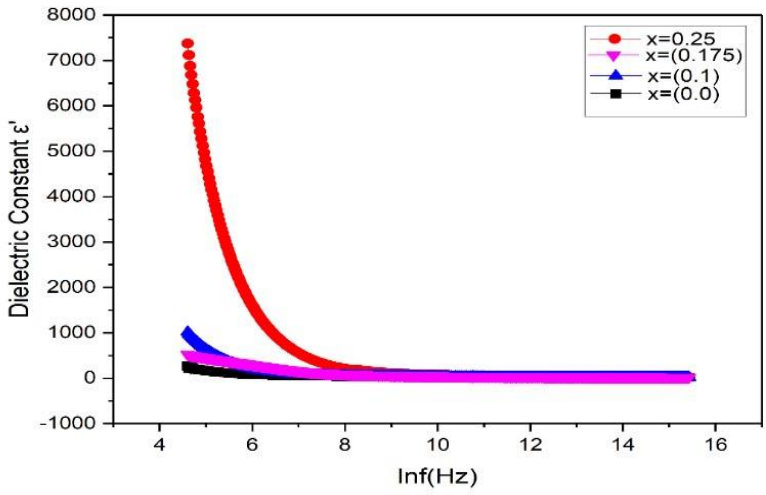


Figure 5.6: Dielectric Constant as a function of frequency

The increase of dielectric constant values at lower frequencies can be well explained by Maxwell and Wagner model of space charge polarization [61]. According to this model, a dielectric material is divided into two parts, grains, and grain boundaries. Grains are relatively conductive while grain boundaries are highly resistive [62]. When an external field is applied, the electrons start to move toward grain boundaries. Accumulation of electrons happens at the grain boundaries because of the resistive nature of boundaries and result in the polarization of material [61]. Accumulation of charge carriers occur at grain

boundaries when the frequency of applied field is low, causing the space charge polarization resulting in high values of dielectric constant. At higher frequencies, a slow response is shown by these charge carries which result in decrease in space charge polarization and ultimately low values of dielectric constant.

Table 5.2: Dielectric Constant values of Pure and Doped.

| **Sample** | **Dielectric Constant** |
|---|---|
| $BaFe_{12}O_{19}$ | $2.29\times10^{2}$ |
| $Ba_{1-2x}$ ($Ni_x$, $Co_x$) $Fe_{12}$ $O_{19}$ (X=0.1) | $6.38\times10^{2}$ |
| $Ba_{1-2x}$ ($Ni_x$, $Co_x$) $Fe_{12}$ $O_{19}$ (X=0.175) | $9.50\times10^{2}$ |
| $Ba_{1-2x}$ ($Ni_x$, $Co_x$) $Fe_{12}$ $O_{19}$ (X=0.25) | $1.45\times10^{3}$ |

With the addition of metallic cations, an increase in dielectric constant can be seen in the figure. Metallic cations will occupy the tetrahedral sites, forcing the $Fe^{+3}$ ions to migrate toward the octahedral site [61]. Hence the electron hoping between $Fe^{+3}$ to $Fe^{+2}$ on the octahedral site will increase resulting in enhanced polarization. Also, the difference in electronegativity value of doped metallic cations and iron is less as compared to barium hence they will donate their electrons to iron resulting in increase of charge carrier. With increased number of charge-carriers the space charge polarization also increases so the dielectric constant will increase with high dopant concentration [62].

### 5.5.2 Dielectric Loss:

The values of dielectric loss are decreasing with increase of frequency. With the increasing addition of dopant, the dielectric loss is seemed to increase. At lower values of frequency, dielectric loss has higher values. Dielectric loss values start to decrease as the frequency of the applied field is increased [65]. Also, with the increasing dopant concentration the value of dielectric loss increased from 90.8 for pure barium hexaferrite to 1790 for barium hexaferrite doped with Ni and Co where x= 0.25. The decreasing behavior of dielectric loss at higher frequencies

can be explained by Koop's theory. According to this theory, polarization requires more energy in low frequency regions because of highly resistive grain boundaries [64]. Hence energy losses are high. Whereas resistivity of grain boundaries in high frequency region is relatively lower so the polarization of material become slight easy. Hence the dielectric losses start to decrease.

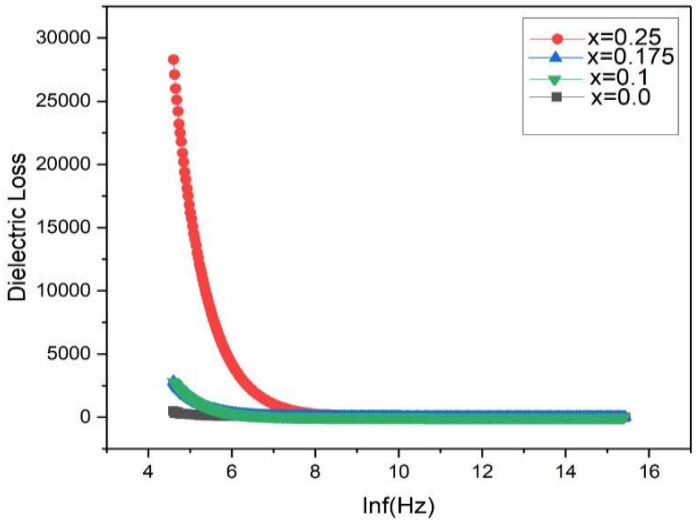


Figure 5.7 Dielectric Loss Variation with frequency.

Table 5.3: Dielectric Loss values of Pure and Doped BaM.

| **Sample** | **Dielectric Loss** |
|---|---|
| $BaFe_{12}O_{19}$ | $9.08\times10^{-1}$ |
| $Ba_{1-2x}$ ($Ni_x$, $Co_x$) $Fe_{12}$ $O_{19}$ (X=0.1) | $5.47\times10^{-2}$ |
| $Ba_{1-2x}$ ($Ni_x$, $Co_x$) $Fe_{12}$ $O_{19}$ (X=0.175) | $1.10\times10^{-3}$ |
| $Ba_{1-2x}$ ($Ni_x$, $Co_x$) $Fe_{12}$ $O_{19}$ (X=0.25) | $1.79\times10^{-3}$ |

With increasing dopant concentration, increase in dielectric loss can be seen in the figure. Movements of charge carriers in the alternating electric field cause the

dissipation of energy and hence the dielectric loss occurs. As the doping concentration is increased, number of charge carrier moving in the alternating electric field also increase causing high dielectric losses [64]. Therefore, dielectric loss is highest for x=0.25 concentration of dopant in barium hexaferrite.

### 5.5.3 Dielectric Tangent Loss:

Tangent loss is given by ratio of complex part of permittivity to real part i.e. Ɛ''/ Ɛ'. Dielectric tangent loss quantifies the relative dissipation of energy due to applied alternating electric field [63]. Figure shows the plot of dielectric tangent loss and natural log of frequency of applied field. At low frequencies, the tangent loss is high because the hopping of electron between Fe+3 and Fe+2 is higher whereas this hopping reduces at higher frequency resulting in decrease of dielectric tangent loss values [65].

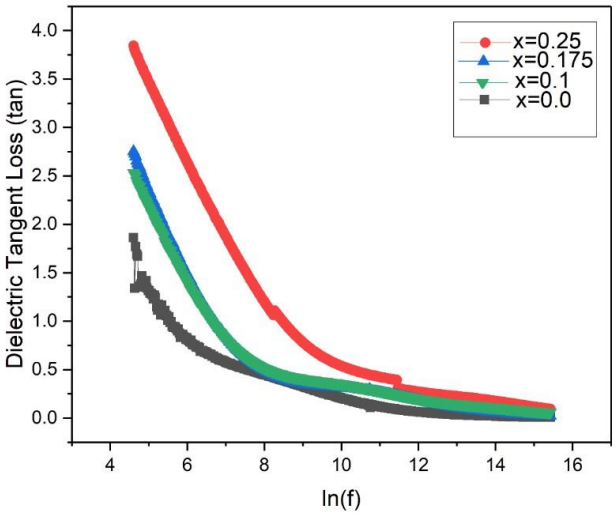


Figure 5.8: Dielectric Tangent Loss variation with frequency.

### 5.5.4 AC Conductivity:

The relation that was used to measure the conductive properties of materials is given below. The measurements were gathered in the range of 1MHz to 1GHz.Fig 5.9. shows increase in AC conductivity with increase in frequency. Max-Well Wagner two lattice model is used to explain this trend of AC Conductivity. At lower frequencies grain boundaries are observed to be more active than higher

frequencies. Therefore, they provide more resistance to the hopping of electrons. But at higher frequencies more active conductive grain boundaries promote to the hopping of electrons [52]. Ac conductivity increases with doping of silver and copper into the ferrite nanoparticles due to conductive nature of both dopants ε' Tan δ here, ω=2πf, permittivity of free space is given by $\varepsilon_o$, and dissipation factor is given by Tanδ & ε' shows the value of dielectric constant. Fig 5.9. shows increase in AC conductivity with increase in frequency. Max-Well Wagner two lattice model is used to explain this trend of AC Conductivity. Therefore, they provide more resistance to the hopping of electrons. But at higher frequencies more active conductive grain boundaries promote to the hopping of electrons [52]. Ac conductivity increases with doping of Nickel and Cobalt into the ferrite nanoparticles due to conductive nature of both dopants.

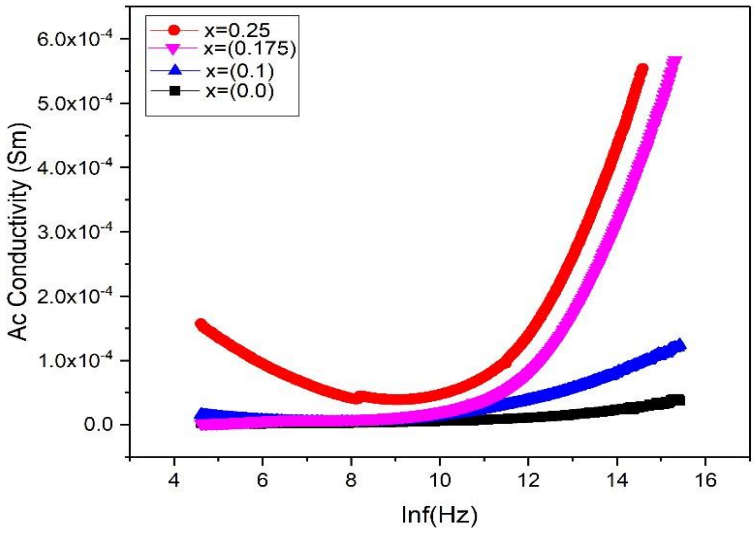


Figure 5.9: Graph showing AC conductivity

### 5.5.5 Impedance:

The total resistance of the system is expressed as Impedance. Relation between frequency and impedance can be observed in figure 5.10. There was decrease impedance by increasing dopant concentration.

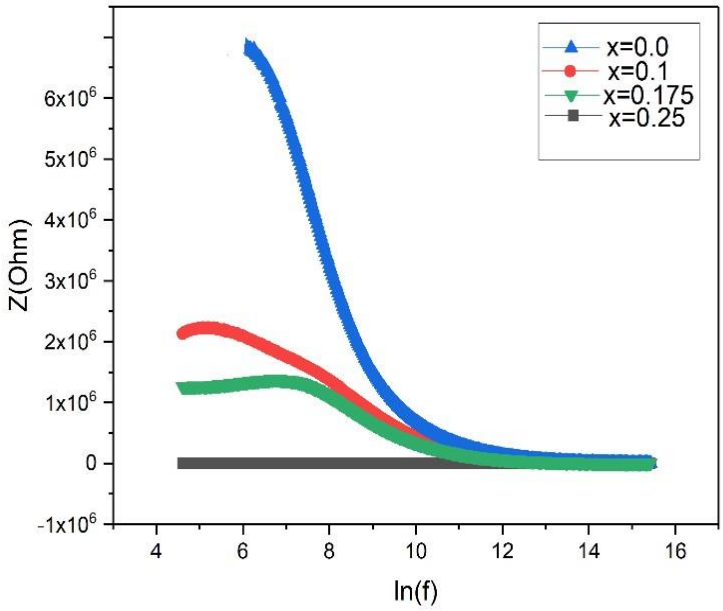


Figure 5.10: Impedance showing total resistance of the system

### 5.5.6 UV Visible Spectroscopy:

Optical spectra for photocatalytic degradation of MB dye in the presence $Ba_{(12x)}Ni_xCo_xFe_{12}O_{19}$ ferrite with composition of x =0.0 (minimum) and x=0.25 (maximum) under visible sun light shown in figure

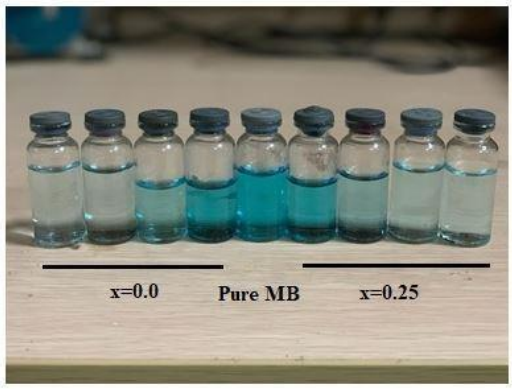


Figure 5.11: Photocatalytic degradation

The figure clarifies the change in the MB color, degradation under visible light in the presence of $Ba_{(1-2x)}Ni_xCo_xFe_{12}O_{19}$ as a catalyst [20]. Solution color changes from dark blue to pale blue during time of photodegradation reaction

increased. During the process of photodegradation the pH value of solution not changed for better adherence.

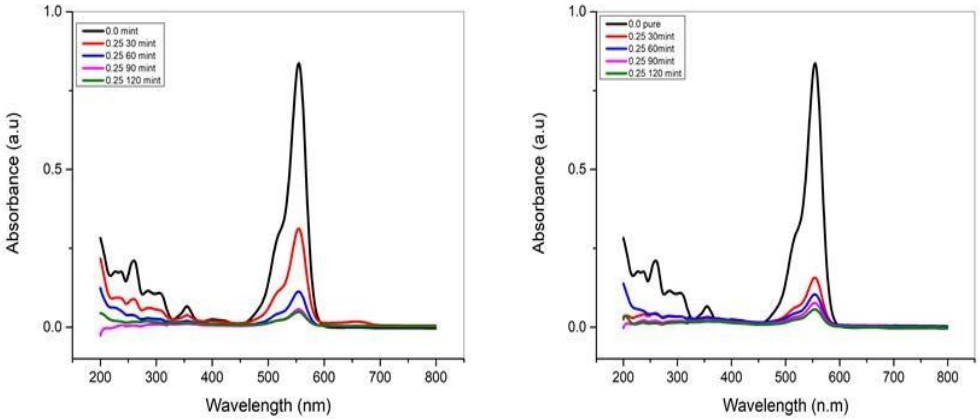


Figure 5.12: Decomposition of Methylene Blue

Above graphs explain the decomposition of MB in the presence of $Ba_{(1-2x)}Ni_xCo_xFe_{12}O_{19}$ powder. The five maximal absorption peaks at 664, 613, 334, 292, 247 nm under typical conditions. The changes in the concentration of MB solution in the presence of hexaferrite powder $Ba_{(1-2x)}Ni_xCo_xFe_{12}O_{19}$ because the band at 664 nm matched well with the bandgap energy of $BaFe_{12}O_{19}$ where the direct $E_g$ was determined at 1.7eV.The intensity of absorption peaks at 664nm seem to be fading with exposing time to sunlight confirming the degradation efficiency. By using the equation $A_t/A_0$ in a place of Ct/Co concentration shown in figure. Both samples showed MB dye degraded upto 80 % with pure Barium ferrite and 90% with cobalt cation and Nickel cation doped Barium ferrite after 120mint. The effect of doping increases the photocatalytic efficiency.

During the irradiation under the direct sunlight the photon energy (hν) greater than the value of $Ba_{(1-2x)}Ni_xCo_xFe_{12}O_{19}$ . At the surface photoexcitation reaction occur, resulting the formation of equal number of holes and electron in valance band (VB) and conduction band (CB). The oxidation reaction occurs at valance band due to photo-generated pairs with $H_2O$ or OH. As from equations:

$$(h\nu) + Ba_{(1-2x)}Ni_xCo_xFe_{12}O_{19} \rightarrow Ba_{(1-2x)}Ni_xCo_xFe_{12}O_{19}\ (e^- + h)$$

$$h_+ + H_2O \rightarrow OH_- + H_+$$

$$h^+ + OH \rightarrow OH^-$$

Reduction process emerges in valance band, the electron reacts with adsorptive species like oxygen on the surface to produced anion superoxide species. The photo-catalytic degradation involves main 3 type oxidant species like hole ($h^+$), superoxide $O_2^-$ / hydroxyl-radicals ($OH^-$) which is primary radicle. Many ways for generation of $OH^-$ radicle.

Reaction of holes with $H_2O$, Holes react with $OH^-$, formation of $H_2O_2$ in intermediate at once disassociate two hydroxyl ions by reacting with photons of light (hv) and superoxide $O_2^-$ and reaction with $O_2$ with photo-generated electrons $e^-$ which reacts with surrounding water to produced hydroxyl radicle (OOH).By increasing the exposure time, generation of electron-holes pair increase which react with generated species hence degradation with time.

Reaction kinetics explained by Langmuir-e-Hinshelwood who give all the reaction involved in photo-catalytic dye degradation.

$$r = -dtdc = \overline{1k + rK\overline{K''CC}} \ldots\ldots\ldots\ldots (5.2)$$

Here $-\frac{dc}{dt}$ degradation rate, $k_r$ is the reaction rate, $K'$ is adsorption coefficient, C is reactance concentration and t is exposure time. After ignoring the denominators terms final equation

$$'C = KC \ldots\ldots\ldots\ldots (5.3)$$

$$r = dt = k_r K$$

Integration and by applying limits to equation we get final equation

$$(\frac{1}{C_t}) - (\frac{1}{C_o}) = Kt \text{……..(5.4)}$$

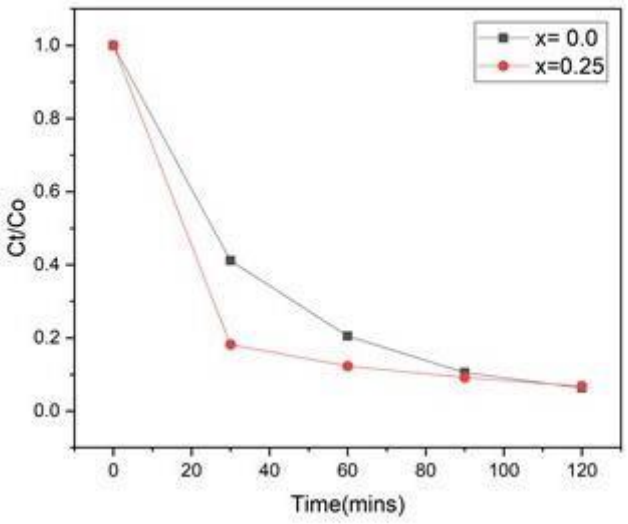


Figure 5.13: Photodegradation

$C_o$ dye concentration at t=0 while Ct after exposure to sun light. The plot of log $(\frac{C_o}{C_t})$ and $(\frac{1}{C_t}) - (\frac{1}{C_o})$ as a function of time. These are probability of first order pseudo equation.

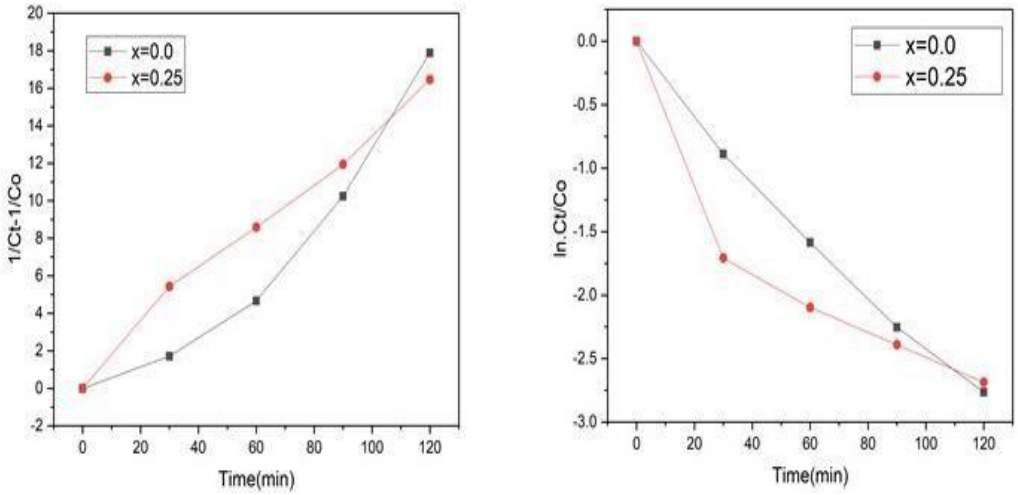


Figure 5.14: Photodegradation/photosynthesis

More likely there are four spectral band of MB arises during the process of photodegradation in the presence of $TiO_2$ or other catalyst. By using $TiO_2$ at catalyst in MB solution, the MB solution degrade into final product by the way through *N*demethylation, deamination, and oxidative degradation during photocatalysis process. By employed $Ba_{(1-2x)}Ni_xCo_xFe_{12}O_{19}$ as a photocatalyst for degradation, the 5-absorption band does not show any shift at irradiation period, but intensity of peaks decreases , explain that there is no intermediate were formed during and photocatalyst degradation process and it could complete in one step. MB degrade into Carbon dioxide, Nitrogen dioxide and $H_2O$. The redox potential of MB degradation is at the bottom of conduction band of $Ba_{(1-2x)}Ni_xCo_xFe_{12}O_{19}$ By transfer of electron from conduction of redox potential level of MB cause degradation of solution into final product in one step. The electronic structure of $BaFe_{12}O_{19}$ have been examined theoretically and experimentally. At the top of valance band, the energy level is 0.0eV and at the bottom of conduction band. All this calculation done by first principal and x-ray emission of photoelectrons. MB has redox potential level at 0.53eV which is below then 1.7eV energy level of conduction band. By transferring of electron from bottom of conduction band of $BaFe_{12}O_{19}$ to the redox potential level of MB which cause MB to get oxidized into inorganic compound. Degradation of MB in the presence of $BaFe_{12}O_{19}$ is different than $TiO_2$ or other photocatalyst.

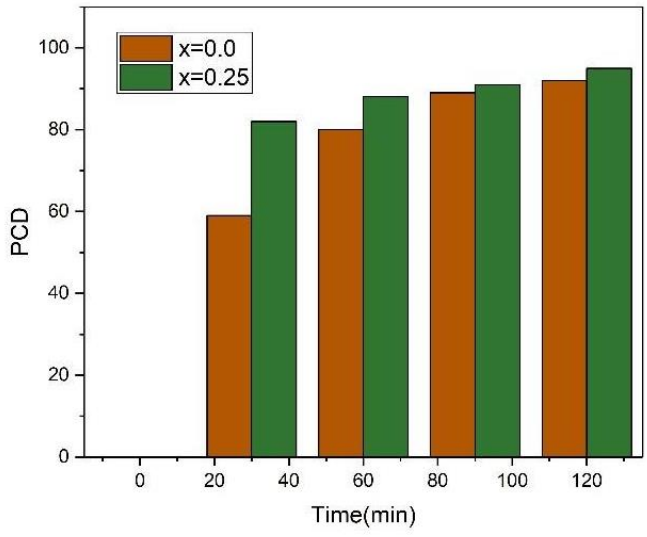


Figure 5.15: PCD Efficiency

The PCD efficiency can clearly see by the fig, with increasing the doping of the cobalt and Nickel cation into Barium degradation efficiency increased. The pure Barium hexaferrite when x=0.0 efficiency about 80% and while doped with cation concentration x=0.25 increased the efficiency about 90% after 120 mints. The band gap of the material is lowering due to cobalt and Nickel cation concentration increased. This narrow band gap increases movement of e from VB to CB. The increase in the concentration increases the generated electron and holes pair's density. OH is mainly the favorite species for degradation process and doping concentration increased the more active sites.

# Conclusions:

The pure and doped Barium ferrite was successfully synthesized by using Sol-Gel method. XRD pattern of $Ba_{1-2x}\,Ni_x\,Co_x\,Fe_{12}O_{19}$ (x= 0, 0.1, 0.175, 0.25) confirm that there was no impurity observed in the prepared samples. Crystallite size was found using Scherer equation which lies within the range of 37-55 nm. SEM images clearly show that prepared nanoparticles were fine, spherical in shape and there was little agglomeration observed. The images of SEM show the particles to be spherical and less agglomerated as the dopant concentration increases. FTIR analysis confirm the presence of metal-oxygen bonds in tetrahedral and octahedral sites of the ferrites and with the addition of dopants, there are band shifts towards lower and higher frequency range which shows the redistribution of cations. The LCR meter was used to study the dielectric properties of prepared ferrites. Dielectric constant shows higher values in lower frequency region while decreases with increasing frequency. AC conductivity also increases with increasing frequency. All the properties like dielectric constant, dielectric loss, tangent loss, AC conductivity trends were in the good agreement with the Maxwell-Wagner model and Koop's theory. Vibrating sample magnetometer (VSM) was used to analyze the magnetic properties of the prepared samples. It has been observed that the saturation magnetization is increases for $Ba_{1-2x}\,Ni_x\,Co_x\,Fe_{12}O_{19}$ with increase in concentration because of higher ionic radii. Magnetic Coercivity studies of the pure and doped sample revealed a decrease in the value of coercivity with dopant. UV-Vis confirms the Photodegradation in the presence of Methyl-Blue the degradation process observed under the sunlight for 0-120mins at the rate of 30mins per sample concentration wise $Ba_{1-2x}\,Ni_x\,Co_x\,Fe_{12}O_{19}$ (x= 0, 0.25).

# Future Work:

- Magnetic Properties of $BaFe_{12}O_{19}$/MWCNTs will be measured and studied.
- Different method of synthesis will be followed to increase the yield of product.
- Different dispersing medium will be used to attain better dispersions and attachment of nanoparticles for better results.
- The prepared nanocomposite will be used in some other matrices to study its properties, for example the prepared nanocomposite will be used in concrete to study its EMI shielding properties.

# References:


[1]. L. Thakur and B. Singh, "History and applications of important Ferrites, "Integrated Research Advances, vol. 1, pp. 11 -13, **(2012).**

[2]. J. Haspers, "Ferrites: Their Properties and Applications," in Modern Materials. vol. 3, ed: Elsevier, (**1962) , pp. 259-341- (2009).**

[3]. V. Verma, J. Kapil, and N. Singh, "Structural, magnetic properties of soft and hard ferrites and their emi shielding application in X-band frequency range," 72. **(2011).**

[4]. International Journal of Engineering Research & Technology (IJERT), **pp. 557560, (2014).**

[5]. R. C. Pullar, "Hexagonal ferrites: a review of the synthesis, properties and applications of hexaferrite ceramics," Progress in Materials Science, vol. **57, pp. 1191-1334, (2012).**

[6]. D. S. Mathew and R.-S. Juang, "An overview of the structure and magnetism of spinel ferrite nanoparticles and their synthesis in microemulsions," Chemical engineering journal, **vol. 129, pp. 51 -65, (2012).**

[7]. N. Gupta, P. Jain, R. Rana, and S. Shrivastava, "Current development in synthesis and characterization of nickel ferrite nanoparticle," Materials Today: Proceedings, **vol. 4, pp. 342- 349, (2017).**

[8]. G. Nabiyouni, M. J. Fesharaki, M. Mozafari, and J. Amighian, "Characterization and magnetic properties of nickel ferrite nanoparticles prepared by ball milling. technique," Chinese Physics Letters, **vol. 27, p. 126401, (2010).**

[9]. R. Valenzuela, "Novel applications of ferrites," Physics Research International, **vol. (2012).**

[10]. R. Mas-Balleste, C. Gomez-Navarro, J. Gomez-Herrero, and F. Zamora, "2D materials: to graphene and beyond," Nanoscale, vol. 3, pp. 20-30, **(2012).**

[11]. D. Li and R. B. Kaner, "Graphene-based materials," Nat Nanotechnol, **vol. 3, p. 101, (2002).**

[12]. D.-H. Chen and X.-R. He, "Synthesis of nickel ferrite nanoparticles by solgel method," Materials Research Bulletin**, vol. 36, pp. 1369-1377, (2012).** Y. Liu, X. X. Liu, and Z. Y. Zhang, "Preparation and Microwave

[13]. Absorption Property of Nickel Spinel Ferrite," in Key Engineering Materials, **(2013)., pp. 36-39**.

[14]. P. A. Noorkhan and S. Kalayne, "Synthesis, Characterization Ac Conductivity of Nickel Ferrite," Journal of Engineering Research and Applications, **vol. 2, pp. 681-685, (2012).68**

[15]. S. Anjum, A. Rashid, F. Bashir, S. Riaz, M. Pervaiz, and R. Zia, "Effect of Cudoped nickel ferrites on structural, magnetic, and dielectric properties," IEEE Transactions on Magnetics, **vol. 50, pp. 1 -4, (2014).**

[16]. K. V. Babu, G. Satyanarayana, B. Sailaja, G. S. Kumar, K. Jalaiah, and M. Ravi, "Structural and magnetic properties of Ni0. 8M0. 2Fe2O4 (M= Cu, Co) nanocrystalline ferrites," Results in Physics**, vol. 9, pp. 55-62, (2011).**

[17]. P. Yin, Y. Deng, L. Zhang, W. Wu, J. Wang, X. Feng, et al., "One-step hydrothermal synthesis and enhanced microwave absorption properties of Ni0.5Co0. 5Fe2O4/graphene composites in low frequency band," Ceramics International, **vol. 44, pp. 20896-20905, (2018).**

[18]. S. A. Soomro, I. H. Gul, M. Z. Khan, H. Naseer, and A. N. Khan, "Dielectric properties evaluation of NiFe2O4/MWCNTs nanohybrid for microwave applications prepared via novel one step synthesis," Ceramics International, **vol. 43, pp. 4090-4095, (2012).**

[19]. S. Akhter, D. P. Paul, M. A. Hakim, D. K. Saha, M. Al-Mamun, and A. Parveen, "Synthesis, structural and physical properties of Cu1 – xZnxFe2O4 ferrites," Materials Sciences and Applications**, vol. 2, p. 1675, (2012).**

[20]. L. Zhang, X. Yu, H. Hu, Y. Li, M. Wu, Z. Wang, et al., "Facile synthesis of iron oxides/reduced graphene oxide composites: application for electromagnetic wave absorption at high temperature," Scientific reports, **vol. 5, p. 9298, (2018).**

[21]. R. Singh, J. Ladol, H. Khajuria, and H. N. Sheikh, "Nitrogen doped graphene nickel ferrite magnetic photocatalyst for the visible light degradation of methylene blue," Acta Chimica Slovenica, **vol. 64, pp. 170-178, (2017).**

[22]. X. Zhao, Z. Zhang, L. Wang, K. Xi, Q. Cao, D. Wang, et al., "Excellent microwave absorption property of graphene-coated Fe nanocomposites," Scientific reports, **vol. 3, p. 3421, (2012).**

[23]. J. Balavijayalakshmi, N. Suriyanarayanan, and R. Jayaprakash, "Role of copper on structural, magnetic and dielectric properties of nickel ferrite nano particles," Journal of Magnetism and Magnetic Materials, **vol. 385, pp. 302-307, (2015).**

[24]. E. R. Kumar, R. Jayaprakash, G. S. Devi, and P. S. P. Reddy, "Magnetic, dielectric and sensing properties of Nickel substituted copper ferrite nanoparticles," Journal of Magnetism and Magnetic Materials, **vol. 355, pp. 87-92, (2014).**

[25]. Z. Wang and Z. Guang-Lin, "Microwave absorption properties of carbon nanotubes-epoxy composites in a frequency range of 2-20 GHz," Open Journal of Composite Materials, **vol. 3, p. 17, (2012).**

[26]. Ž. Cvejić, S. Rakić, S. Jankov, S. Skuban, and A. Kapor, “Dielectric Properties of Nanosized ZnFe2O4,” Process. Appl. Ceram. , vol. 2, no. 1, pp. 53–56, **(2008).**

[27]. R. S. Totagi, R. B. Pujar, and S. B. Koujalagi, “Synthesis, characterization, study of electrical properties and survey of applications of Nano ferrites-an approach by chemical method,” **vol. 6, no. 3, pp. 272–279, (2014).**

[28]. M. Shen, S. Ge, and W. Cao, “Dielectric enhancement and Maxwell Wagner effects in polycrystalline ferroelectric multilayered thin films,” J. Phys. D. Appl. Phys., **vol. 34, no. 19, pp. 2935–2938, (2012).**

[29]. R. Denton and N. W. Ashcroft, “Vegard’s law,” Phys. Rev. A, **vol. 43, no. 6, pp. 3161 –3164, Mar. (1991).**

[30]. E. Ciomaga et al. , “Preparation and magnetoelectric properties of NiFe2O 4-PZT composites obtained in-situ by gel-combustion method,” J. Eur. Ceram. Soc. , **vol. 32, no. 12, pp. 3325–3337, (2012).**

[31]. H. Gul and E. Pervaiz, “Comparative study of NiFe2-xAlxO4ferrite nanoparticles synthesized by chemical co-precipitation and sol-gel combustion techniques,” Mater. Res. Bull. , **vol. 47, no. 6, pp. 1353–1361, (2018).**

[32]. T. T. N. Vu, G. Teyssedre, S. Le Roy, and C. Laurent, “Maxwell–Wagner Effect in Multi-Layered Dielectrics: Interfacial Charge Measurement and Modelling,” Technologies, **vol. 5, no. 2, p. 27, (2019).**

[33]. M. Ajmal and A. Maqsood, “Structural, electrical and magnetic properties of Cu1-xZnxFe2O4ferrites ($0 \leq x \leq 1$),” J. Alloys Compd., vol. 460, no. 1 –2, pp. **(2011).**

[34]. S. H. Kareem, "Synthesis of Polyethylene of Glycol-coated Nickel Zinc Ferrite and Polyvinyl Alcohol-coated Nickel Zinc Ferrite Nanoparticles Via CoPrecipitation Method," **(2018).**

[35]. H. M. Khan, "Effect of Divalent and Trivalent Cations on the Electrical and Magnetic Properties of Hexa-ferrites," **(2016).**

[36]. L. A. Vaughan, "Vaughan, L. A. (2011). Environmentally benign synthesis and application of some spinel ferrite nanoparticles," **(2018).**

[37]. M. R. Rehman, "Improvement of electrical properties of strontium hexaferrite nanoparticles by substitution of cobalt," **(2016).**

[38]. S. U. Marwat, "Effect of MWCNTs on Structural and Dielectric Properties of Cobalt Substituted Nickel Ferrite," **(2019).**

[39]. E. a. A. V. Spain, "Spain, E., & Venkatanarayanan, A. (2014). 13.02 Review of Physical Principles of Sensing and Types of Sensing Materials.," **(2018).**

[40]. V. &. M. V. Marghussian, "Magnetic properties of nano-glass ceramics. Nanoglas ceramics," **(2015).**

[41]. S. &. A. E. SHAMEBO, "Studies on Structural, Electric, Dielectric and Magnetic Properties of Nickel-Based Ferrite Materials". **(2014).**

[42]. P. V. C. F. &. B. P. Coutinho, "Structural, vibrational and magnetic properties of the orthoferrites LaFeO3 and YFeO3: A comparative study. Solid State Communications**," (2018).**

[43]. N. P. Solanki, "Crystal structure and preparation techniques for Hexaferrite".

[44]. P. S. R. J. G. Kajal K. Mallick ∗, "Dielectric properties of M-type barium hexaferrite," **(2013).**

[45]. M. Sugimoto, "The Past, Present, and Future of Ferrites," 1999. b. E. G. S. H. Y.J. W. D. L. K.S. Martirosyana, "Barium hexaferrite nanoparticles: Synthesis and magnetic properties**," (2011).**

[46]. S. S. R. P. L. K. P. a. Sunil Kumara), "Crystal Structure and Magnetic Properties of Cr Doped," **(2018).**

[47]. M. R. M. H. M. Radwan ∗, "Microstructure and magnetic properties of Aldoped barium ferrite," **(2013).**

[48]. Y. n. Y. Daming Chen, "Microstructure and magnetic properties of Aldoped barium ferrite," **(2013).**

[49].n. H. H. A. H. Sözeria, "Magnetic, dielectric and microwave properties of M–Ti substituted barium hexaferrite," **(2014).**

[50]. S. R. Pratap Behera, "Effect of Ni doping on structural, magnetic and dielectric properties of M type barium hexaferrite**," (2018).**

[51]. H. M. M. B. G. H. &. A. R. S. Hossein Nikmanesh, "Synthesis of multi-walled carbon nanotube/doped barium hexaferrite nanocomposites: An investigation of structural, magnetic and microwave absorption properties," Ceramics International, **(2019).**

[52]. S. Y. M. &. M. A. Mesdaghi, "The effect of PANI and MWCNT on magnetic and photocatalytic properties of substituted barium hexaferrite nanocomposites," Materials Chemistry and Physics, **(2018).**

[53]. R. S. M. M. &. N. H. Alam, "Influence of Multi-Walled Carbon Nanotubes (MWCNTs) Volume Percentage on the Magnetic and Microwave Absorbing Properties of BaMg0. 5Co0. 5TiFe10O19/MWCNTs Nanocomposites," Materials Research Bulletin, **(2016).**

[54]. V. C. S. S. E. M. M. L. K. R. H. &. M. S. S. Chavan, "Transformation of hexagonal to mixed spinel crystal structure and magnetic properties of Co2+ substituted BaFe12O19," Journal of Magnetism and Magnetic Materials, 398, 32-37., **(2016).**

[55]. K. K. S. P. &. G. R. J. Mallick, "Magnetic properties of cobalt substituted M type barium hexaferrite prepared by co-precipitation.," Journal of Magnetism and Magnetic Materials, **(2007).**

[56]. M. G. &. S. S. C. Shalini, "Magnetic studies of cobalt doped barium hexaferrite nanoparticles prepared by modified sol-gel method.," AIP Conference Proceedings, **(2016).**

[57]. M. R. M. A. M. T. A. K. F. A. K. A. A. M. S. &. S. M. Waqar, "Synthesis and properties of nickel-doped nanocrystalline barium hexaferrite ceramic materials.," Applied Physics , **(2018).**

[58]. V. B. M. P. S. V. S. G. &. C. E. Galstyan, "Metal oxide nanostructures in food applications: Quality control and packaging.," Chemosensors, **(2018).**

[59]. S. E. W. D. J. S. S. M. M. L. &. L. S. Shirsath, "Ferrites obtained by sol-gel method," **(2018).**

[60]. R. B. D. P. S. U. &. S. B. G. Sharma, "X-ray diffraction: a powerful method of characterizing nanomaterial," Recent Research in Science and Technology, (**2012)**.

[61]. R. S. S. F. C. M. K. R. M. D. M. A. S. &. S. F. S. M. Melo, "Magnetic ferrites synthesized using the microwave-hydrothermal method," Journal of Magnetism and Magnetic Materials, (**2015).**

[62]. L. L. X. H. X. X. Z. T. D. J. Z. F. &. H. C. Yuan, "Flexible solid-state supercapacitors based on carbon nanoparticles/MnO2 nanorods hybrid structure," ACS nano, **(2012)**.